A long-term dataset of debris-flow and hydrometeorological observations from 1961 to 2024 at Jiangjia Ravine, China

Li Wei [1], Dongri Song[1, 2], Peng Cui[1], Lijun Su[1], Gordon G. D. Zhou[1], Kaiheng Hu[1], Fangqiang Wei[3], Yong Hong[1], Guoqiang Ou[1], Jun Zhang[1], Zhicheng Kang[1, †], Xiaojun Guo[1], Wei Zhong[1], Xiaoyu Li[1], Yaonan Zhang[2,4], Chao Shi[5], Hui ~~Tang~~[5]Tang[6]

[1] Institute of Mountain Hazards and Environment, Chinese Academy of Sciences, Chengdu 610213, China

[2] National Cryosphere Desert Data Center, Lanzhou 730000, China

[3] Chongqing Institute of Green and Intelligent Technology, Chinese Academy of Sciences, Chongqing 400714, China

[4] Northwest Institute of Eco-Environment and Resources, Chinese Academy of Sciences, Lanzhou 730000, China

[5]School of Civil and Environmental Engineering, Nanyang Technological University, 639798, Singapore

[~~5~~ [6] Earth Surface Process Modelling, German Research Centre for Geosciences (GFZ), Potsdam, Germany

† deceased

Correspondence: Dongri Song (drsong@imde.ac.cn)

Abstract: The study of mechanisms of debris-flow formation and movement is constrained by the lack of comprehensive and long-term field monitoring data. In 1961, the Dongchuan Debris Flow Observation and Research Station (DDFORS) was established in the highly active debris-flow catchment of Jiangjia Ravine to conduct continuous field observations of debris flows. With the advancement of technology, more high-precision instruments have been employed to monitor the entire process of debris flows. This paper presents a unique and comprehensive dataset of debris flow and hydrometeorological observations collected over a 64-year period (1961-2024) at Jiangjia Ravine, China. The dataset documents 17,001 surges for a total of 278 debris-flow events, encompasses detailed measurements of kinematic parameters of debris flow, including velocity, depth, and discharge, as well as physical-mechanical parameters such as particle size distribution of debris flow, yield stress, and viscosity of debris-flow slurry. It also incorporates the induced seismic data, providing insights into the dynamic characteristics of debris flows. Furthermore, it includes continuous records of rainfall at minute intervals, soil moisture, and suspended sediment concentrations at the catchment scale. This extensive dataset provides invaluable insights into the initiation, transportation, and deposition processes of debris flows. It can be utilized to analyze flow resistance and dynamic characteristics of debris flows, to validate various computational models, to investigate the effects of debris flows on channel morphology, and evaluate the impact of climate change on sediment transport within watersheds. The dataset is publicly accessible through the National Cryosphere Desert Data Center (NCDC) (https://www.ncdc.ac.cn/) and is organized into several categories to facilitate ease of use and analysis.

1. Introduction

Debris flows are catastrophic mass movement phenomena that occur in mountainous regions, characterized by their multiple surges, high velocity, high-concentration of sediment, and destructive potential. These events pose a significant threat to human lives, infrastructure, and the natural environment. In-situ debris-flow observation is crucial for improving our understanding on the triggering condition (run-off generated, or landslide transition, etc.), flow dynamics, as well as for the development, calibration and validation of debris-flow models (Berti et al. 2000; Marchi et al. 2002; Cui et al. 2005; McCoy et al. 2010; Suwa et al. 2011; Coviello et al., 2015). Direct field observations yield real-time data that capture the physical attributes and behavior of debris flows, such as flow velocity, sediment concentration, and flow depth, which are not fully obtainable through remote sensing or modeling alone (LaHusen, 2005; Arattano and Marchi, 2008; Hübl and Mikoš, 2018; Hürlimann et al., 2019).

Several catchments prone to debris flows are equipped with observation systems. In the European Alps, these include Lattenbach Creek and Wartschenbach Catchment in Austria (Hübl and Moser, 2006; Hübl and Kaitna, 2010; Fuchs et al., 2012; Hübl et al., 2017), ~~Erlenbach Torrent,~~ Illgraben Catchment, Dorfbach Torrent, and Spreitgraben Catchment in Switzerland (~~Rickenmann and McArdell,2007;~~ McArdell et al., 2007; Berger et al., 2011; ~~Hürlimann et al., 2011, 2015;~~ Tobler et al., 2014; Willi et al.,2015; Hirschberg et al., 2021; Aaron et al.,2023; Raffaele and Jordan, 2024), Moscardo Torrent, Acquabona Creek, and Gadria Basin in Italy (Berti et al., 1999; Genevois et al., 2000; Marchi et al., 2002; Comiti et al., 2014; Blasone et al., 2015; Theule et al., 2018), and Manival Torrent and Réal Torrent in France (Navratil et al., 2013; Theule et al., 2015; Bel et al., 2015). In the European Pyrenees, observation stations are located at Rebaixader Torrent and Portainé Catchment in Spain (Abancó et al., 2014; Hürlimann et al., 2013). In Asia, stations are situated at Kamikamihorizawa Creek on Mount Yakedake in Japan (Suwa et al., 1993; Okano et al., 2012; Ikeda et al., 2023), Shenmu Village and Yushui ~~Stream~~ River (Yin et al., 2011; Liu and Wei, 2024), and Jiangjia Ravine in the Xiaojiang River Catchment in China. Additionally, the Chalk Cliffs in Colorado Rocky Mountains in the United States are continuously monitored (Pierson ,1986; Coe et al., 2010; McCoy et al., 2011, 2012). Most debris-flow monitoring systems have been operational for less than 30 years.

Table 1 Characteristics of typical monitoring sites

Catchment	Country-Region	Year of installation	Maximum altitude (m asl)	Drainage area (km²)	Main channel length (km)	Reference
Lattenbach	Austria	2002	2930	5.3	5.2	Hübl and Moser, 2006;Hübl and Kaitna, 2010; Hübl et al., 2017
Wartschenbach	Austria	1995	2113	2.7	3.6	Fuchs et al., 2012
Illgraben	Switzerland	2000	2716	11.7	5.5	McArdell et al., 2007; Berger et al., 2011; Hirschberg et al., 2021; Aaron et al.,2023; Raffaele and Jordan, 2024
Dorfbach	Switzerland	1993	4545	5.6	3.2	Willi et al.,2015
Spreitgraben	Switzerland	2009	3263	4.7		Tobler et al., 2014
Moscardo	Italy	1989	2043	4.7	2.76	Marchi et al., 2002; Blasone et al., 2015

Acquabona	Italy	1997	2667	0.3	1.6	Berti et al., 1999; Genevois et al., 2000;
Gadria	Italy	2011	2945	6.3	3	Comiti et al., 2014; Theule et al., 2018
Manival	France	2010	1738	3.6	1.8	Theule et al., 2015; Bel et al., 2015
Réal	France	2010	2090	2.3	2.6	Navratil et al., 2013
Rebaixader	Spain	2009	2475	0.53	1.4	Abancó et al., 2014
Portainé	Spain	2015	2439	5.72	5.7	Hürlimann et al., 2013
Kamikamihorizawa	Japan	1970	2455	0.8	2.5	Suwa et al., 1993; Okano et al., 2012; Ikeda et al., 2023
Chalk Cliffs	USA	2004	3140	0.3	1	Pierson ,1986; Coe et al., 2010; McCoy et al., 2011, 2012
Shenmu	Taiwan, China	2002	2850	72.2	17.7	Yin et al., 2011
Yushui River	Taiwan, China	2018	2756	12.3	7.31	Liu and Wei, 2024
Jiangjia Ravine	China	1961	3269	48.6	13.9	

Despite the extensive investment on debris-flow monitoring, the availability of publicly accessible debris-flow datasets remains limited (Lapillonne et al., 2023). Among these datasets, notable examples include those from the Moscardo Torrent, Dorfbach Torrent, Spreitgraben Catchment, Lattenbach Creek, and Illgraben Catchment. Marchi et al. (2018) compiled a dataset encompassing 809 debris-flow events across 537 basins in the mountainous regions of northeastern Italy from the mid-19th century to 2016, including debris-flow volume, year of occurrence, drainage basin area, and the geographical coordinates of the basin outlets. Marchi et al. (2021) later provided debris-flow hydrographs and rainfall data for 30 events recorded in the Moscardo Torrent between 1990 and 2019. Mitchell et al. (2022) published records of discharge, flow depth, and velocity for 11 debris flow events in the Dorfbach Torrent, one event in the Spreitgraben Catchment, and 9 events at Lattenbach Creek. McArdell and Hirschberg (2020) documented dates and bulk volumes of 75 debris-flow events at the Illgraben Catchment from 2000 to 2007, while McArdell et al. (2023) extended this with debris-flow characteristics including occurrence date and time, peak-flow depth, peak-flow velocity, total volume, and bulk density for the period 2019-2022. Hirschberg et al. (2024) contributed volumetric water content measurements, water level, and pressure data for a location along the Illgraben debris-flow channel during the 2022 debris-flow season. Fan et al. (2019) recorded the debris-flow events and their triggering rainfall that occurred from 2008 to 2017 in Longmen Mountains after the 2008 Wenchuan earthquake, parts of event were with detailed discharge, flow depth and density. Wang et al. (2022) provided date of 186 debris flows and triggering rainfall induced by the 2008 Wenchuan earthquake.

In addition, several published academic articles provide data sheets detailing the dynamic characteristics of debris-flow events. For example, Theule et al. (2018) presented dynamic parameters of debris-flow surges based on LSPIV measurements, visual feature analyses from orthorectified images, and radar sensor data collected in 2011, 2013, 2014, and 2015. Lapillonne et al. (2023) summarized hydraulic features such as the Froude regime, velocity, flow level, and discharge for 35 debris-flow surges gathered between 2011 and 2020 in the Réal torrent Catchment. Comiti et al. (2014) provided the main characteristics of three debris flows occurred in the Gadria basin from 2011 to 2013. Additionally, Marchi et al. (2002, 2021) reported debris-flow velocity, peak discharge, and volume for 30 events between 1990 and 2019.

89　　　　Overall, the majority of available datasets pertains to parameters of individual debris-flow events.
90　There is a notable absence of long-term datasets that include both dynamic process characteristics and
91　physical-mechanical parameters, which are essential for a comprehensive dynamic analysis of debris-
92　flow processes. Continuous field observations of debris flow at the highly active Jiangjia Ravine
93　catchment commenced in 1961 and continue to be conducted by the Dongchuan Debris Flow Observation
94　and Research Station (DDFORS) (Zhang, 1993; Cui et al., 2005; Hu et al., 2011). The station was initially
95　established by the Dongchuan Mining Bureau to mitigate the impacts of debris flows on river blockages
96　and damage to the transportation infrastructure of the copper mines. It was later taken over by the Chinese
97　Academy of Sciences in 1972. These observations in the station focus on the initiation, transportation,
98　and deposition processes of debris flows. The data collected at this observatory now spans 64 years,
99　including starting-ending moments, velocity, depth, discharge, bulk density, particle size distribution,
100　yield stress, and viscosity. In addition to these parameters, long-term measurements of rainfall, cross-
101　sectional elevation, and other meteorological variables such as soil moisture and suspended sediment
102　content have also been recorded. Furthermore, seismic, and video footage on debris flows have been
103　collected in recent years. This dataset records detailed flow characteristics of debris-flow surges, rather
104　than merely the parameters of individual debris flow events. This 64-year dataset documents 17,001
105　surges for a total of 278 debris-flow events, with maximum surge flow discharge and volume recorded
106　at 8,026 m³/s and 249,112 m³, respectively.

107　　　　This paper summarizes of the debris-flow observation at Jiangjia Ravine and provides an overview
108　ofoverviews of the core data, including kinematic parameters, seismic data, particle size distribution,
109　yield stress, viscosity, and other related measurements. We begin by introducing the study area and then
110　describe the methods used for data collection and processing. Illustrative examples of the dataset are
111　provided to demonstrate its utility. Finally, we review several studies that have utilized this dataset and
112　conclude with information on how to access the full dataset.

2. Study area

2.1 Geology

115　　　　The Jiangjia Ravine is located on the right side of the Xiaojiang River, Yunnan Province in China.
116　The coordinates of the ravine are between 103°05′46″-103°13′01″E and 26°13′16″-26°17′13″N. The
117　elevation ranges from 1088 m a.s.l. to a maximum of 3269 m a.s.l. with an area of 48.6 km^2 and a main
118　gully length of 13.9 km. It is situated within the Xiaojiang fault zone, one of the most active fault systems
119　on the southeastern margin of the Tibetan Plateau. The region is characterized by active neotectonic
120　movements and intense seismic activity. The rocks are intersected by three fault systems trending north-
121　south, northeast, and northwest (Wu et al., 1990). This region is characterized by intense neotectonic
122　activity, resulting in frequent and severe earthquakes, with magnitude IX to X events occurring almost
123　every century. The sandstone and slate within this area are weak, highly susceptible to weathering, and
124　easily to be fragmented. Approximately 80% of the exposed rocks are highly fractured and slightly
125　metamorphosed, serving as the primary source of material for debris flows (Zhang et al., 2023).

2.2 Geomorphology

127　　　　The topography of the watershed is higher in the east (with the highest elevation of 3269 m) and
128　lower in the west (with the lowest elevation of 1042 m). The shape of the watershed is wider in the east
129　(about 7 km) and narrower in the west (about 2 km). The watershed is characterized by high mountains
130　and steep slopes, with a relative elevation difference of approximately 500 meters between the ridges
131　and valleys (Fig.1a). Areas with slopes exceeding 25° and 35° make up 55% and 16% of the total

watershed area, respectively (Cui et al., 2005). The Jiangjia Ravine contains more than 200 tributary gullies, including 154 incised gullies and 46 gullies. The main channel is divided into three sections, each with distinct morphological characteristics: (1) the erosion area, also known as the debris-flow triggering zone, is 6.5 km long with an average slope of 11°; (2) the transportation area, 2.6 km long with an average slope of 4.9°, and (3) the deposition area, 4.8 km long, has an average slope of 3.7°. With the siltation of sediment in the main channel, the deposition area keeps increasing, while the transportation area keeps decreasing.

2.3 Climate

The climate of Jiangjia Ravine is characterized by distinct dry and wet seasons, along with a pronounced vertical climatic zonation (Chen, 1985). It can be divided into three climatic zones: (1) the subtropical dry-hot valley region, located at elevations below 1600 m a.s.l.; (2) the subtropical and warm temperate subhumid region, situated between 1600 and 2200 m a.s.l.; and (3) the temperate humid mountain region, found at elevations above 2200 m a.s.l. (Guo et al., 2012).The rainy season extends from May to October, during which more than 85% of the annual rainfall occurs, while the dry season lasts from November to April, receiving less than 15% of the yearly total (Scott and Wang, 2003). Heavy rains and thunderstorms are frequent in the rainy season, contributing to more than half of the annual precipitation. The heaviest rainfall typically occurs between 2500 m and 3000 m a.s.l. Annual precipitation in the watershed increases with elevation, while evaporation decreases with rising elevation (Chen et al., 2011).

2.4 Soil and vegetation

The underlying soils in the region include torrid red soil, red soil, brown soil, yellow soil, and mountainous brown soil, corresponding to different zones. Croplands are mainly distributed on gentler hillslopes (<25°) near the divides and on the alluvial fan. Some steeper hillslopes are covered by sparse shrubs or grass, while the others are barren for frequent failures (Yang et al., 2022).

Due to the weak lithology, crisscrossing faults, steep terrain, and sparse vegetation in the watershed, landslide, and collapse activities are intense, covering an area that accounts for 61% of the total watershed, storing 1.23 billion cubic meters of loose solid materials (Fig.1b). Weathering-derived debris accounts for 70-80% of the loose material sources, while loose sedimentary deposits constitute 20-30% of the total (Li and Wu, 1981). During the rainy season, debris flows frequently occur, with each event consisting of tens to hundreds of surges (Fig. 2a). These surges, known as surge flows, are characterized by a distinct head and body. Surge flows are typically separated by periods of flow interruption or quiescence. In contrast, when a debris flow persists for an extended period without noticeable surge features（such as a pronounced head), it is classified as a continuative flow.These surges, known as surge flows, are characterized by a distinct head, body, and tail. In contrast, continuous flows lack these well-defined phases (Kang et al., 1990). The ravine, now known as the "debris-flow museum" in China, offers optimal research conditions. It is the site where China's earliest prototype observation and research on debris flows were initiated, primarily to address the recurring river blockages caused by debris flows (up to 10 blockages in the year 1961) (Wu et al., 1990) (Fig.2b). Initially, basic observation devices were installed in 1961, followed by the early-stage infrasound monitoring of debris flows (Zhang et al.,2004). Over the past 64 years, the site has developed into a comprehensive field laboratory for automated observation, experimentation, and instrument validation (Fig. 1c). More information of DDFORS and its debris-flow monitoring can be found in Cui et al. (2005) and Kang et al. (2004).
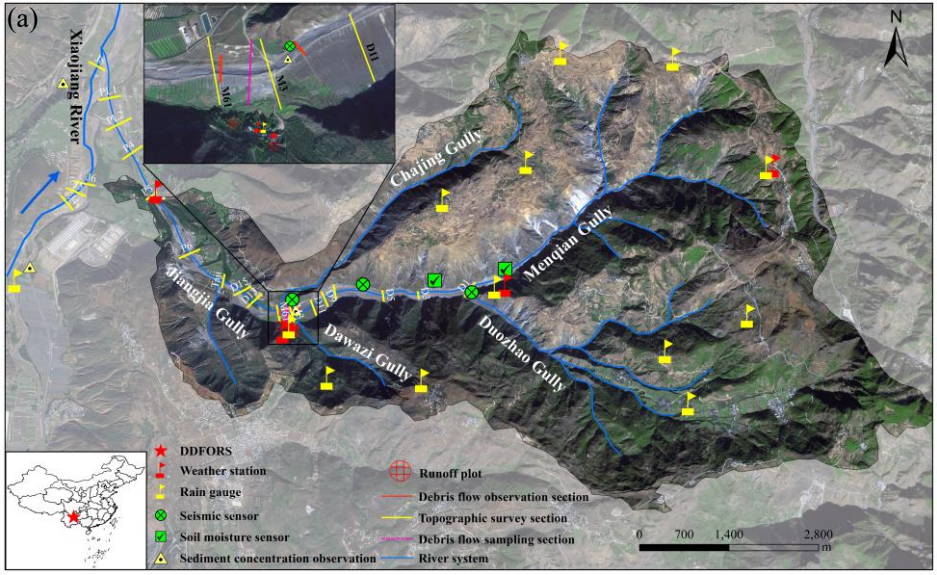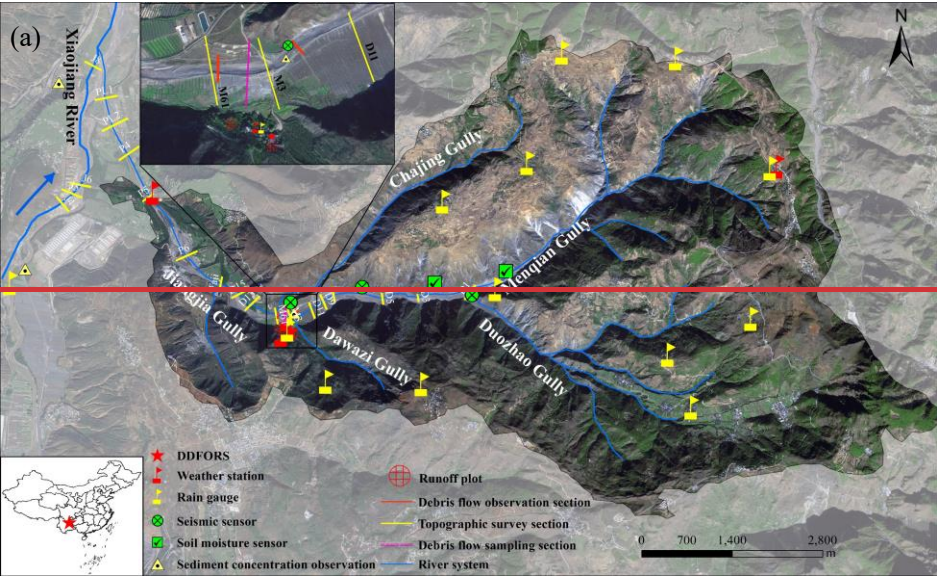
174

175

176

(c)

Figure 1. Photos of observation systems, Jiangjia Ravine and station: (a) ~~The~~ the observation systems at Jiangjia Ravine, satellite image obtained from https://data.cresda.cn/#/2dMap, last access: 3 March, 2025. (b) aerial view of Jiangjia Ravine, with localized heavy rainfall captured in the higher elevation (The terrain is deformed). (~~b~~c)~~,~~ aerial view of Dongchuan Debris Flow Observation and Research Station (DDFORS).


(a)

(b)

Jiangjia Gully

Xiaojiang River

7

Figure 2. Debris flows at Jiangjia Ravine: (a) debris flow erode the channel bank (Photos by Shunli Chen) and (b), (c) confluence of debris flows into the Xiaojiang River.

3. Data

The dataset comprises multiple parameters, including debris-flow kinematic data, rheological, particle size distribution data, seismic data, debris-flow video, cross-section elevation data; meteorological, rainfall, soil moisture, and temperature data; sediment concentration and runoff data from plots; suspended sediment data. The dataset comprises, but not limited to, the data from three published paper-based datasets (in Chinese), containing debris-flow observation records from 1961 to 2000 (Zhang and Xiong, 1997; Kang et al., 2006; Kang et al., 2007). Figure 1a indicates the locations of sampling or monitoring. The specific coordinates of the monitoring location can be found in the dataset. Figure 3 summarizes these datasets along with their respective acquisition periods. The majority of the data were collected at Jiangjia Ravine, while additional sediment flux, rainfall, and meteorological data were also acquired at Xiaojiang River Catchment. The instruments and measurement methods employed are detailed in Table 12.
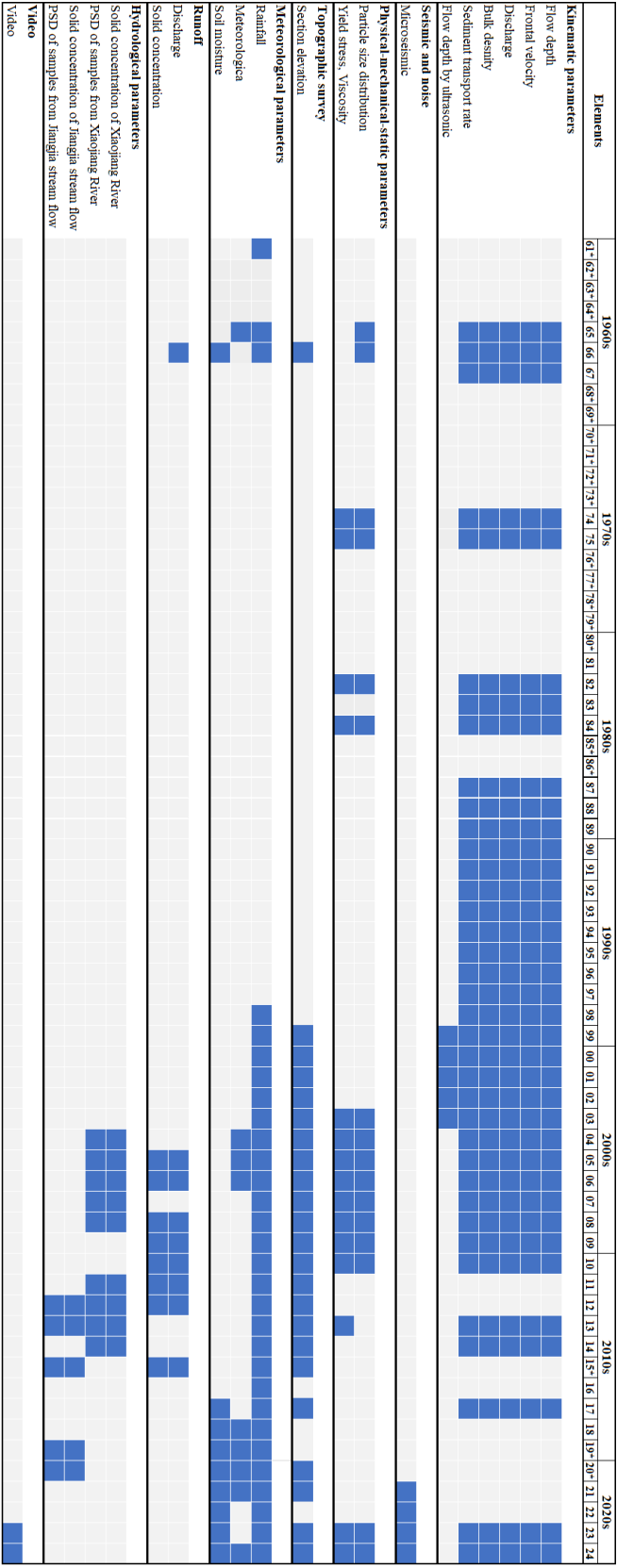
Note: Acquisition period for each parameter is shown in blue. * Denotes debris flows occurred without observational data.

Figure 3. An overview of the dataset.

204
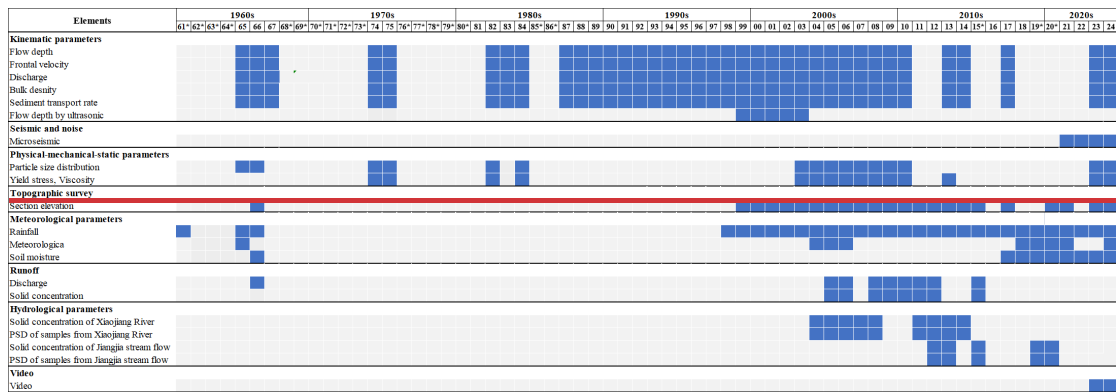
Figure 3. An overview of the dataset.

Table 1 2 Observation parameters and sensor configurations.

Types	Elements	Parameter	Instrument	Manufacturer	Frequency Sampling interval	Accuracy	Resolution
Debris flow	Kinematic parameters	Flow depth	Determined referring to cross section marks and debris-flow level				
		Flow depth by ultrasonic level meter	Ultrasonic sensor	Siemens Milltronics Process Instruments Inc., Germany	10 Hz	±0.25% of the range or 6 mm, whichever is greater	0.1% of the range or 2 mm, whichever is greater
		Surface width	Determined referring to channel width				
		Frontal velocity	Determined by measure distance divided by measure time				
	Seismic	Microseismic	Seismic sensor	Di GOS Potsdam GmbH, Germany	100 Hz		
	Static parameters	Particle size distribution	Particles larger than 0.25 mm analyzed by sieve analysis method. Particles smaller than 0.25 mm analyzed by pycnometer method before 2004. Marvin Laser Particle Size Analyzer (model MS2000) utilized from 2004.	Malvern Panalytical Ltd, UK			
		Yield stress, Viscosity	Rheometer, concentric cylinder system, outer cylinder diameter 43.4 mm, inner cylinder diameter 31.44 mm.	Thermo Electron, Gmbh, Germany			
	Video	Video footage	8 Megapixel 1/1.8 CMOS Intelligent Zoom Bullet	Hangzhou Hikvision Digital			Main Stream specifications: frame rate 25 fps

10

			Network Camera	Technology Co., Ltd, China			Resolution 3840 x 2160, at 50 Hz
	Topography	Section elevation	Level gauge, Real-Time Kinematic	Sichuan Leituo Technology Development Co., Ltd., China		Horizontal direction: ±8mm+1×10^{-6}D; Vertical direction: ±15mm+1×10^{-6}D	
Meteorological parameters	Meteorological parameters	Rainfall	Siphon rain gauge (before 2006), Tipping-bucket rain gauge (2006-2023), Piezoelectric rain gauge (2024)	Shanghai Meteorological Instruments Factory Co., Ltd., China (before 2024); Insentek technology co. ltd, China (2024)	1 min	±0.05 (before 2006); ±0.04 (2006-2023); ±4% (2024)	0.1 mm
		Weather station	Cumulus automatic weather station	ELE International Centre of Excellence Bedfordshire, UK	1 h		
			Weather station	Insentek technology co. ltd, China	1 h	Temperature: ±0.15; Humidity: ±3%; Wind speed: ±2%; Wind direction: ±2°; Atmospheric pressure: ±2°; Solar radiation: ±5%	Temperature: 0.02℃; Humidity: 0.05%RH; Wind speed: 0.01m/s; Wind direction: 0.1°; Atmospheric pressure: 0.1 hPa; Solar radiation: 1W/m^2
Soil moisture	Soil moisture	Soil moisture	Moisture sensor	Dalian Zheqin Technology Co., Ltd., China	1 Hz	±2% within the range of 0-53%; ±4% within the range of 53-100%	
Runoff plot	Runoff	Runoff volume	Measured manually				
		Solid concentration	Analyzed using oven drying method				
Water sample	Hydrological parameters	Solid concentration	Analyzed using the oven drying method				
		Particle size distribution of suspended sediment	Determined by Marvin Laser Particle Size Analyzer (model MS2000)	Malvern Panalytical Ltd, UK			

3.1 Debris flow

3.1.1 Kinematic parameters

Measurement

The debris-flow kinematic parameters were monitored in a straight channel adjacent to the DDFORS (Fig.4). The location of two debris-flow observation sections is shown in Fig. 1a. Observation distances ranged from 50 m to 200 m. Flow time between the two sections was measured using a second chronograph. Depth, defined as the surge front height, was determined by referencing cross-sectional marks on the channel banks, representing the vertical distance between the top of the debris-flow surge

217 and the channel surface (Fig. 4c). Surface width of debris flow was determined by referencing of channel
218 width. Velocity was calculated by dividing the observation distance by the flow time for each surge as it
219 passed through the cross sections. Bulk density of each surge was determined either through sampling
220 weighting or estimation.

221   During 1999-2001, the flow depth of specific debris-flow surges was simultaneously measured using
222 an Airanger SPL ultrasonic level meter installed directly above the channel with a sampling frequency of
223 10 Hz (Fig. 4b). The measurement range extends from 0.3 m to 60 m. The depth value is calculated as
224 the difference between the installation height of the ultrasonic sensors, set at 10 m, and the measured
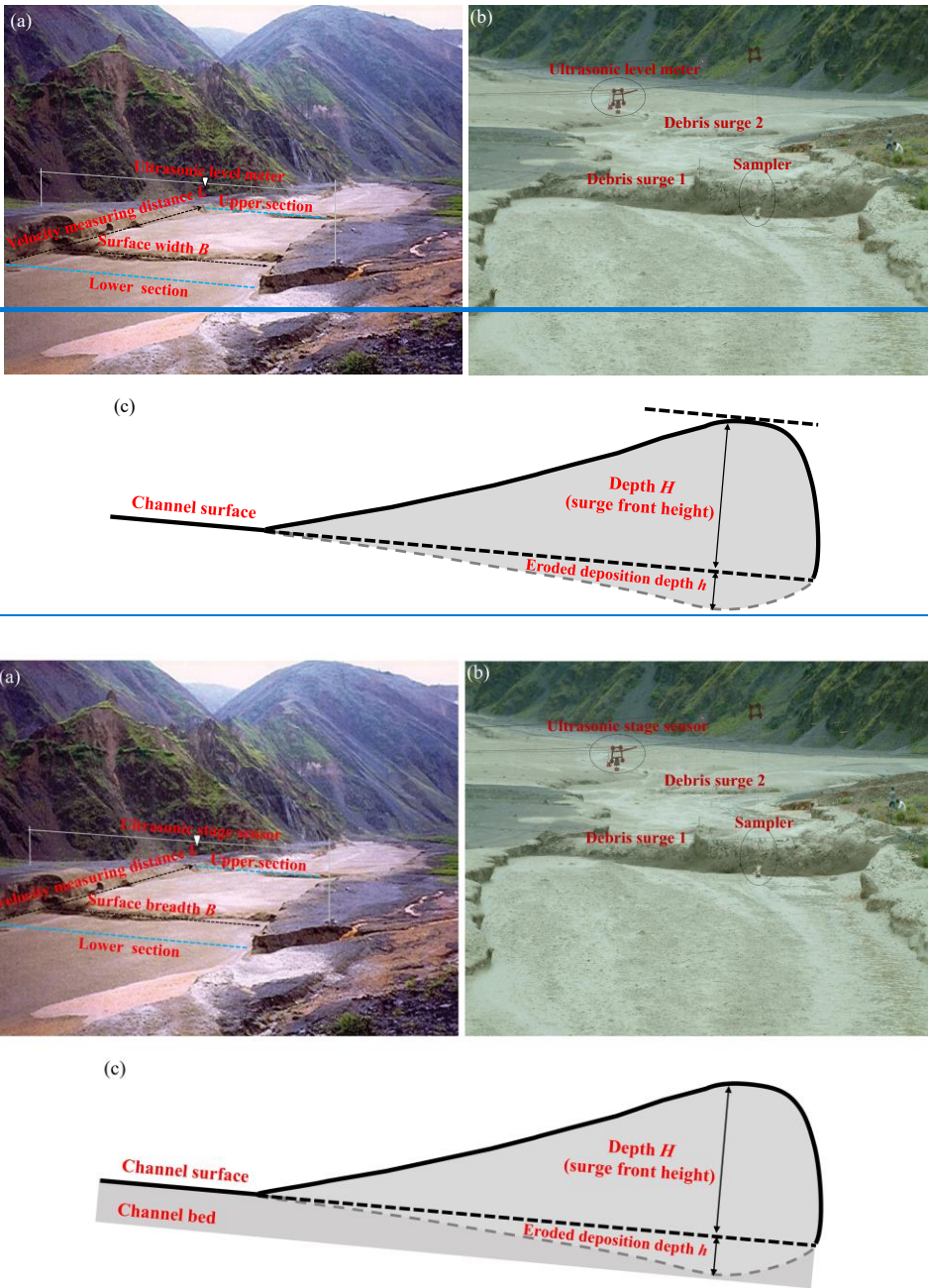225 values.

Figure 4. Field observation of debris-flow kinematics and sampling:(a) (b) surface width, depth and velocity measurement, and (c)illustration of flow depth.

12

230 **Data processing**

231 The discharge, volume, sediment concentration, sediment volume, and sediment transport rate of

232 debris-flow surge were determined based on the observational parameters. A rectangular channel cross

233 section was assumed.

234 The surge discharge Q (m³/s) was calculated as following:

235 $$Q = V \times B \times H \tag{1}$$

236 where V is velocity (m/s), B is surface width (m), and H is surge depth (m).

237 Surge flow volume W_c (m³) was calculated as following:

238 $$W_c = Q \times \frac{T}{2} \quad \text{for surge flow} \tag{2}$$

239 $$W_c = Q \times T \quad \text{for continuative flow} \tag{3}$$

240 where $-T$ is the record time (duration) of debris-flow surge (s), which is the time for surge front minus

241 the time for surge rear. Flow depth hydrograph of surge flow exhibits a triangular shape, so the factor 1/2

242 is applied in the calculation.

243 Sediment concentration S (kg/m³) and volume concentration of debris flow C_v are obtained as

244 following:

245 $$S = \gamma_s \bar{r_s} \times C_v \tag{4}$$

246 $$C_v = \frac{\gamma_c - \gamma}{\gamma_s - \gamma} \tag{5}$$

247 where γ, γ_c, γ_s are ~~unit weight~~density of water, debris flow, and sediment (grain density) respectively;

248 γ_s is taken as 2650 (kg/m³).

249 Sediment volume W_s(m³) and sediment transport rate Q_c (t/s) are calculated as following:

250 $$W_s = W_c \times C_v \tag{6}$$

251 $$Q_c = Q \times S/1000 \tag{7}$$

252 Example of kinematic parameters of debris-flow surges occurred on 7th June, 2013 are presented in

253 Table ~~2~~3. In addition, statistics of debris-flow surge parameters such as total sediment transport volume

254 and total runoff volume are also provided.

255 **Table ~~2~~3** Example of kinematic parameters of debris-flow surges occurred on 7th June, 2013.

No.	Type	Time for surge front T_1 /(h:m:s)	Time for rear of surge T_2 /(h:m:s)	Duration T/s	Surface width B/m	Surge front height H/m	Velocity measuring distance L/m	Time for velocity measurement t/s	Front velocity V/(m/s)	Discharge Q/(m³/s)	~~Unit weight~~Density γ_c/(t/m³)	Sediment transport rate Q_c/(t/s)	Runoff Volume W_c/(m³)
1	Surge flow	03:45:27	03:45:37	10	30.0	0.500	200	42.70	4.68	70.2	2.2000	135.24	351
2	Surge flow	03:46:15	03:46:27	12	50.0	1.000	200	29.65	6.75	337.5	2.2300	666.29	2025

3	Surge flow	03:47:26	03:47:36	10	50.0	0.700	200	34.78	5.75	201.2	2.2000	387.61	1006
4	Surge flow	03:48:40	03:48:52	12	50.0	0.500	200	33.33	6.00	150.0	2.2000	288.98	900
5	Surge flow	03:51:29	03:51:42	13	50.0	0.600	200	40.03	5.00	150.0	2.2000	288.98	975
6	Surge flow	03:54:25	03:54:35	10	50.0	0.700	200	36.83	5.43	190.0	2.2200	372.08	950
7	Surge flow	03:55:02	03:55:13	11	50.0	0.800	200	31.44	6.36	254.4	2.2000	490.10	1399
8	Surge flow	03:56:13	03:56:27	14	25.0	0.500	200	41.39	4.83	60.4	2.2000	116.36	423
9	Surge flow	03:56:40	03:56:51	11	30.0	0.500	200	46.10	4.34	65.1	2.2000	125.42	358
10	Surge flow	03:57:28	03:57:38	10	30.0	0.500	200	44.93	4.45	66.8	2.2000	128.69	334
11	Surge flow	03:58:41	03:58:52	11	50.0	1.000	200	35.63	5.61	280.5	2.2200	549.30	1543
12	Surge flow	03:59:44	03:59:55	11	30.0	0.600	200	50.67	3.95	71.1	2.2000	136.97	391
13	Surge flow	04:00:13	04:00:26	13	50.0	0.600	200	37.98	5.27	158.1	2.2000	304.58	1028
14	Surge flow	04:01:40	04:01:57	17	50.0	1.000	200	28.00	7.14	357.0	2.2500	717.11	3034
15	Continuative flow	04:02:31	04:04:50	139	8.0	0.600	200	43.56	4.59	22.0	2.1500	40.63	3058
16	Continuative flow	04:04:50	04:10:00	310	5.0	0.600	200	33.63	5.95	17.9	2.1500	33.06	5549
17	Continuative flow	04:10:00	04:13:28	208	6.0	0.500	200	28.91	6.92	20.8	2.1500	38.42	4326
18	Continuative flow	04:13:28	04:13:35	7	8.0	0.600	200	33.48	5.97	28.7	2.1500	53.01	100
19	Continuative flow	05:00:00	05:32:00	1920	4.0	0.500	200	47.38	4.22	8.4	2.1500	15.51	16128
20	Continuative flow	05:36:14	05:36:27	13	10.0	0.500	200	43.54	4.59	22.9	2.1500	42.30	149

Note: Time are provided in China Standard Time (CST, UTC+8).

Example of results

The kinematic characteristics of debris-flow surges provide critical information for understanding their behavior and impact. Between 1965 and 2024, a total of 278 debris-flow events were recorded, including 14,887 surge flows and 2,114 continuative flows. These events predominantly occur during the monsoon season, from May to September, with the highest frequency observed in June (55 events), July (113 events), and August (98 events).

14

Cumulative distribution functions of depth-flow depth, discharge, and volume for surge flows and continuative flows were depicted in Fig.5. Maximum flow depth is 5.5 for surge flow and 2.7 for continuative flow (Fig.5a; quantiles at 25%, 50%, and 75% of 0.29 m, 0.39 m, and 0.49 m for surge flows, respectively; quantiles at 25%, 50%, and 75% of 0.50 m, 0.80 m, and 1.2 m for continuative flows, respectively). The discharge of surge flows ranges from 0.5 to 8,026 m³/s, while that range from 0.3 to 1,800 m³/s for continuative flows (Fig.5b; quantiles at 25%, 50%, and 75% of 67.7 m³, 7,063 m³/s, and 1,0594 m³ /s for surge flows, respectively; quantiles at 25%, 50%, and 75% of 4.9 m³, 13.3 m³/s, and 36.3 m³/s for continuative flows, respectively). The volume of surge flows ranges from 2 to 249,112 m³, while that range from 3.4 to 825,600 m³ for continuative flows (Fig.5c; quantiles at 25%, 50%, and 75% of 3,344 m³, 6,673 m³, and 10,009 m³ for surge flows, respectively; quantiles at 25%, 50%, and 75% of 522 m³, 1,043 m³, and 1,564 m³ for continuative flows, respectively).

Figures 6 illustrates examples of measured debris-flow depth, velocity, discharge, and runoff volume of events that occurred on July 16th, 1999. The flow depth measured by ultrasonic level meter, velocity, discharge, and volume exhibit strong fluctuations, with the maximum flow depth and velocity reaching up to 5.4 m and 10.6 m/s, respectively. The volume of debris flow ranged from 403 m³ to 74,615 m³. The maximum values represent the volume of the continuative flow, which has a long duration and typically occurs during the final period of the event.

Figure 7 presents the measured annual sediment volume from 1966 to 2024. During this period, debris flows transported 43.3 million m³ of sediment. Sediment mainly deposited in the main channel, while a portion was transported to the Xiaojiang River. The most substantial debris flows occurred in 1991, transporting 6.69 million m³ of sediment. Overall, the frequency and magnitude of debris flows have significantly declined in recent decades. However, the events in 2023 and 2024 still recorded significant sediment transport volumes of 52,682 m³ and 31,450 m³ , respectively, which remain substantial for mountainous watersheds. The decreasing trend may be a result of climate change. Since 2005, the volume of sediment transported has exhibited a decreasing trend.
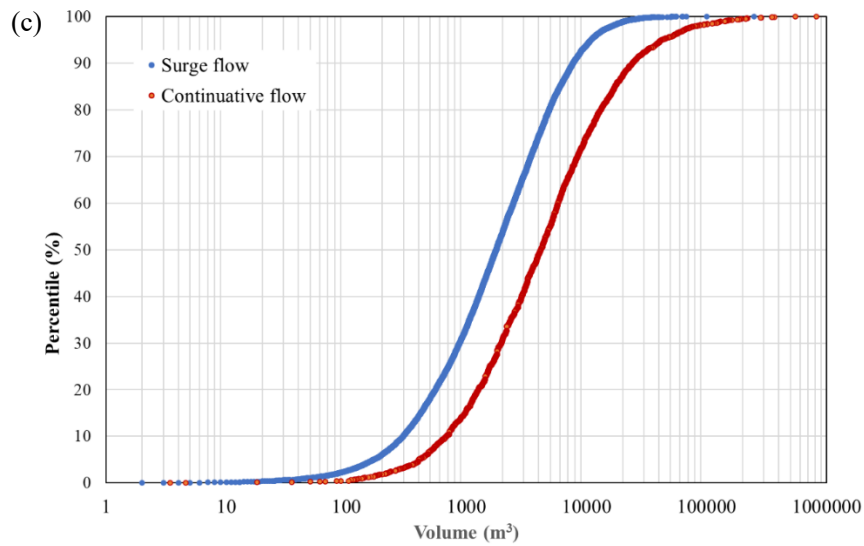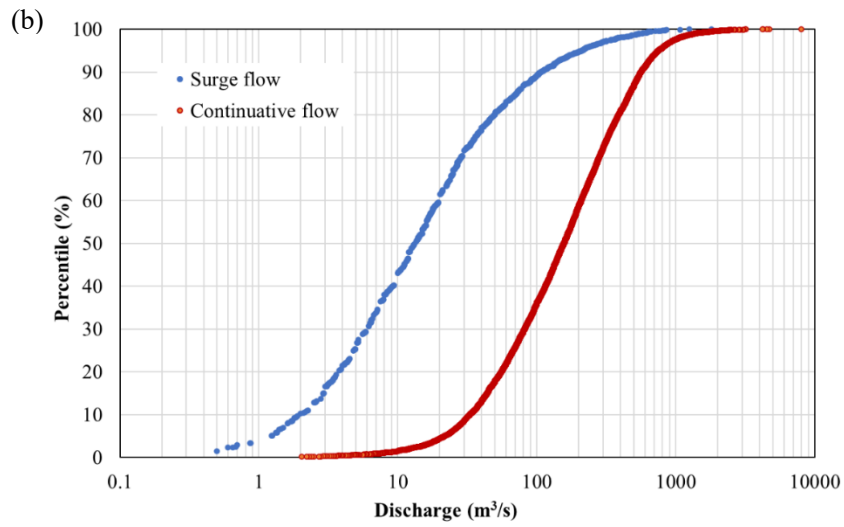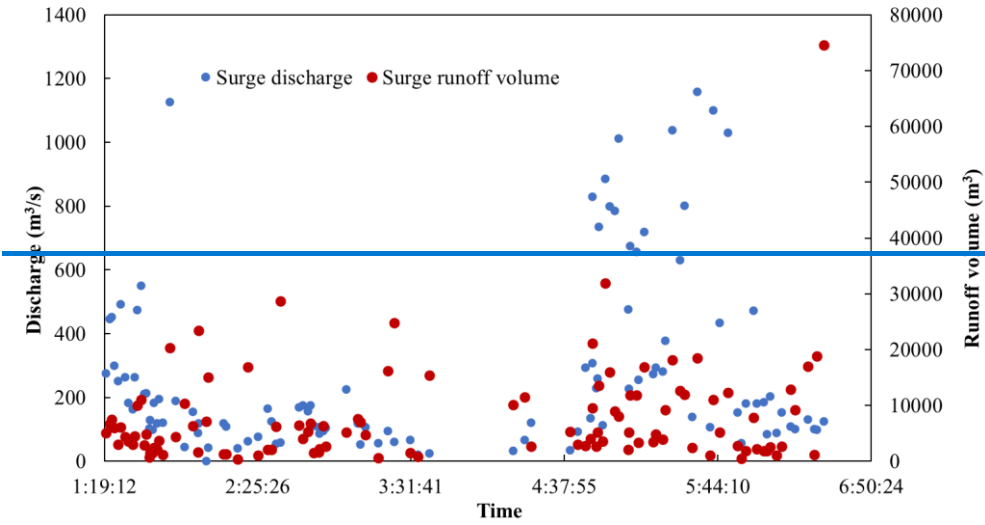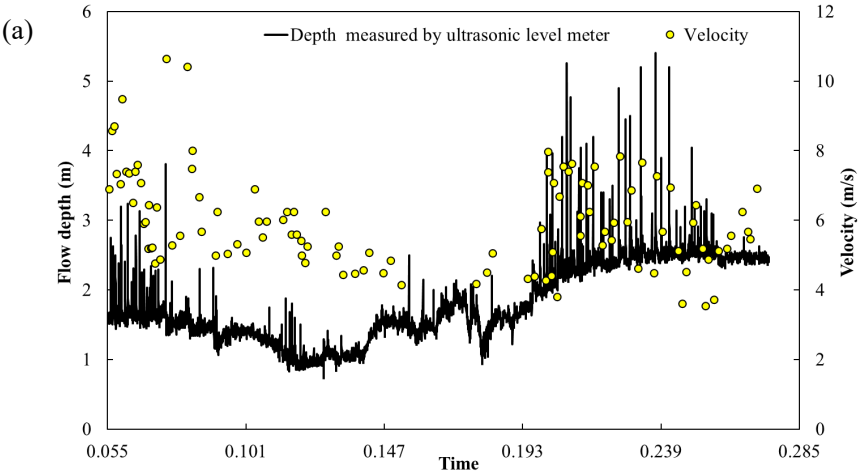
(a)

15

(b)

290

(c)
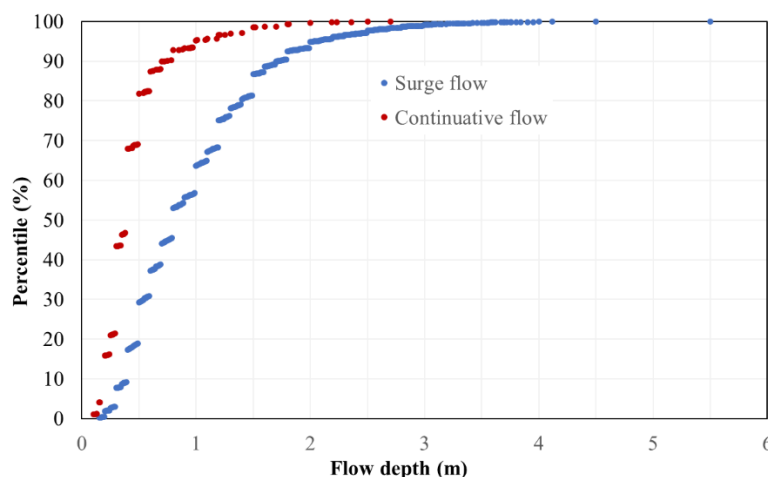
291
292   **Figure 5.** Cumulative density functions of (a) flow depth, (b) discharge, and (c) volume.
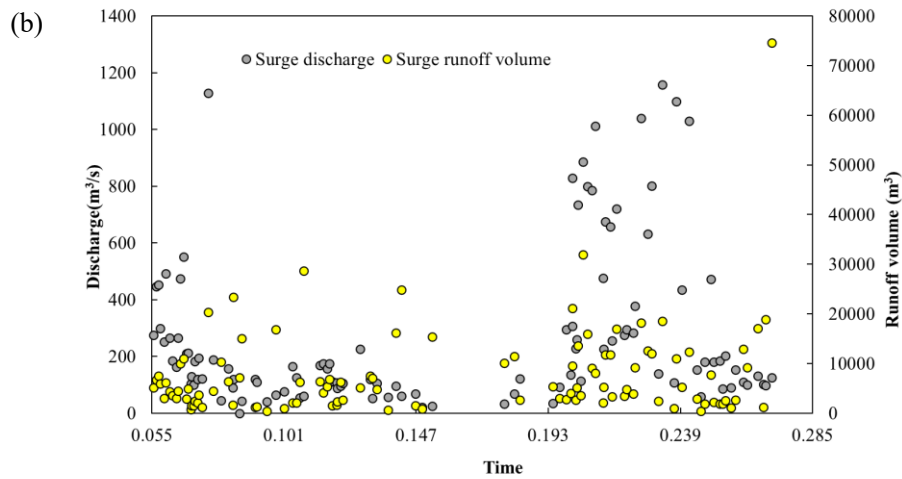
293

(a)

294

295

17

(b)
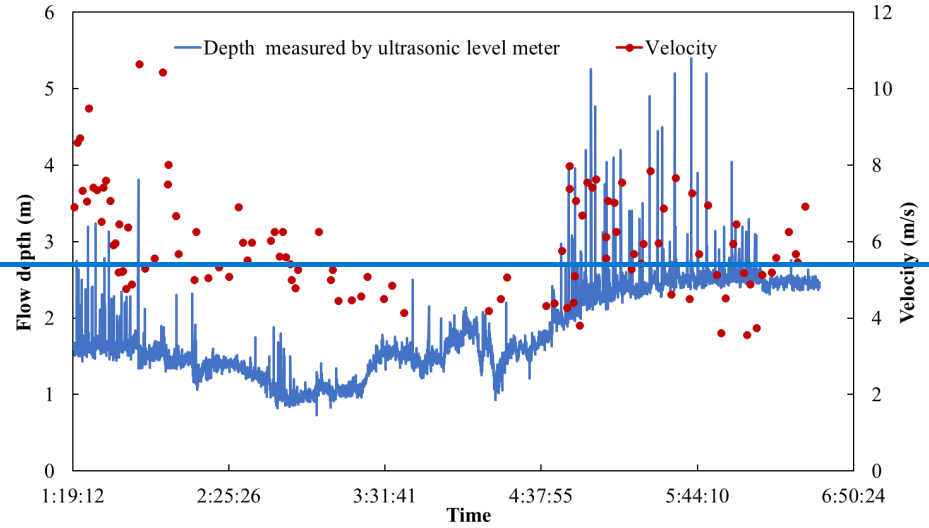
Figure 6. (a) Variation of flow depth, velocity and (b) discharge, volume of debris-flow surges occurred on July 16th, 1999.
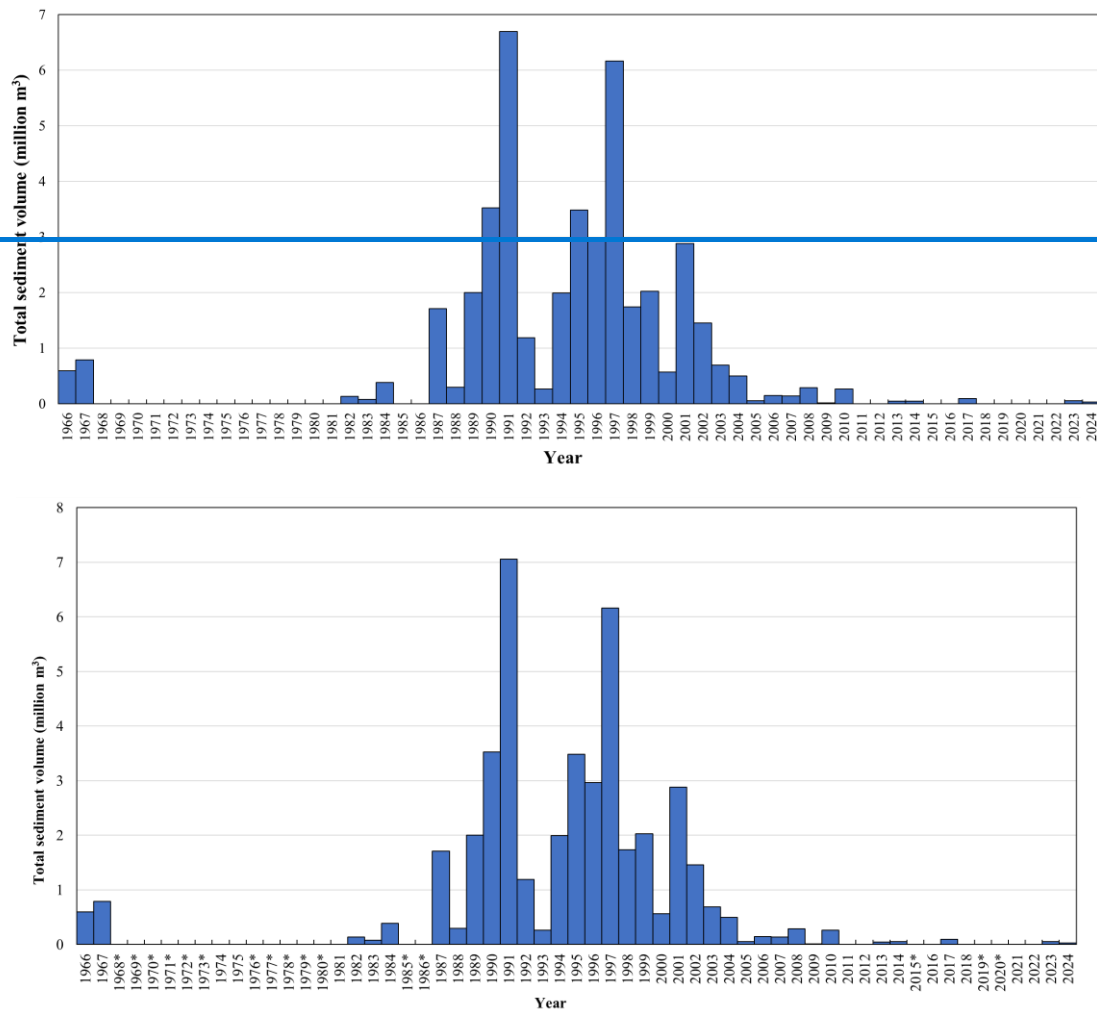

Figure 7. Variation of sediment transported by debris flow recorded from 1966 to 2024. * denotes debris flows occurred without observational data.

18

3.1.2 Seismic data

Measurement

The ground seismic response induced by debris flows was monitored by DATA-CUBE 3-channel seismic recorder. The sensors contain three geophones for different directions and were installed in three locations with average distance of 1.1 km along the main channel within the transportation area (Fig.1a, Fig.8a). The recorded seismic data was stored in the data logger of the sensors, and download manually after the debris-flow events.

Example of results

Figure 8b illustrates the time-domain seismic signal and time-frequency characteristics of the debris-flow event that occurred on July 28th, 2024. The event began at approximately 11:24 (UTC+8) and ended at 12:04 (UTC+8), lasting a total of 40 minutes.

From the time-domain waveforms and time-frequency spectra of seismic signals in the east-west (E-W), north-south (N-S), and vertical (Z) directions, the initiation and cessation of the debris flow are clearly identifiable. A distinct increase in signal amplitude is observed starting around 11:25, peaking at approximately 12:00, which corresponds to the main surge of the debris flow. After this peak, a significant attenuation of the seismic signal is noted post 12:00, indicating a decrease in flow intensity and the eventual cessation of the debris flow.
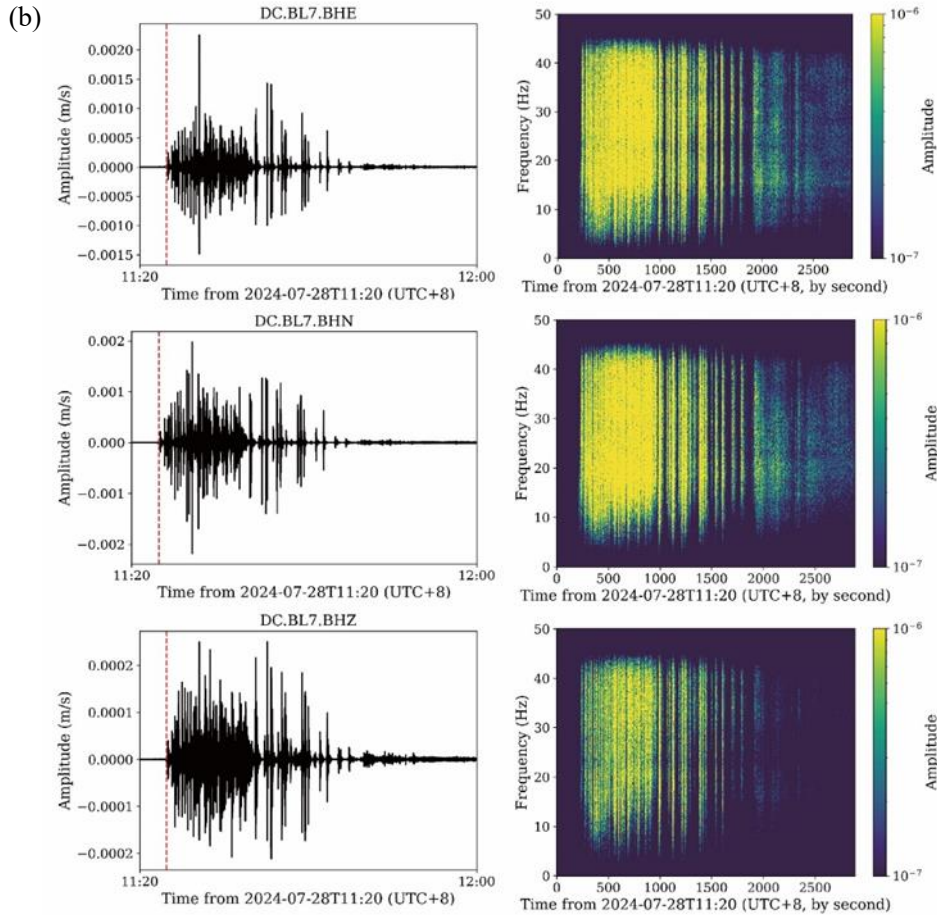
(b)
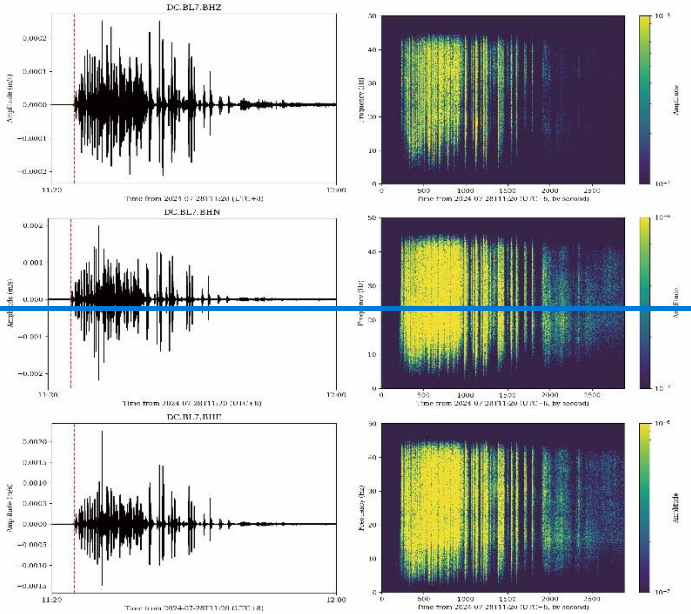
Figure 8. (a) Installation of seismic sensor and (b) the time-domain seismic signal and time-frequency characteristic curves of the debris-flow event on July 28th, 2024.

3.1.3 Particle size, yield stress, and viscosity

Measurement

Debris-flow samples are collected by suspending cable sampler or manual sampling. The cable sampling is collected from the moving surges with a bucket that has a diameter of 190 mm and a volume of 0.012 m^3 (Fig.9). Manual sampling collects the debris-flow deposition near the channel bank by using a circular or square bucket with a volume of 0.0155 m^3 or 0.009 m^3, respectively.

The sample is air-dried and sieved through a steel mesh for particle size analysis. For sediments larger than 0.25 mm, the particle size is determined using the sieve analysis method. For particles smaller than 0.25 mm, the pycnometer method was employed for particle size distribution analysis before 2004. Since 2004, the Marvin Laser Particle Size Analyzer (model MS2000) has been used.

Figure 9. Details of debris-flow sampling.

The yield stress and viscosity of the debris-flow slurry (particles smaller than 1.2 mm) were obtained using a Thermo Haake RS600 Rheometer, which employs a concentric cylinder system. This system features an outer cylinder diameter of 43.4 mm and an inner cylinder diameter of 31.44 mm. The debris-flow slurry sample, containing particles smaller than 1.2 mm, had a volume of 50.5 ml. Measurements were conducted using a Z31 rotor, which is 15.72 mm in diameter and 55 mm in height.

Example of results

Figure 10a illustrates the grain size distribution of debris-flow deposition samples collected from 1974 to 2024. The bulk densities of the samples range from 2,026 kg/m³ to 2,470 kg/m³, with median grain sizes range from 2 mm and 30 mm. Additionally, Figure 10b depicts the rheological curves of two debris-flow slurries during 2004 to 2004, which have bulk densities range from 1,665 kg/m³ to 2,100 kg/m³. The shear stress increases rapidly at lower shear rates, whereas at higher shear rates, the increase becomes more gradual.
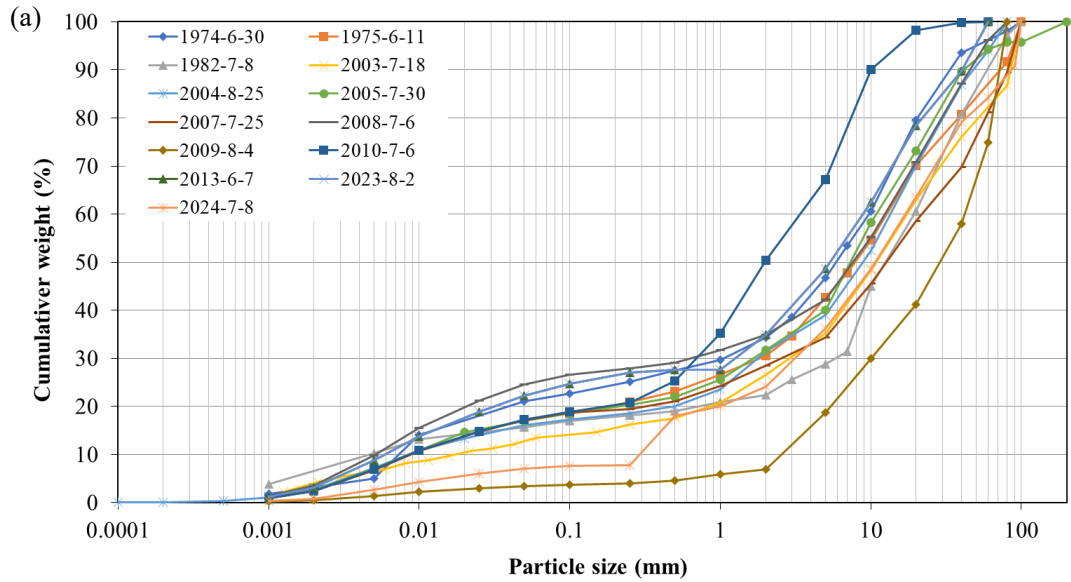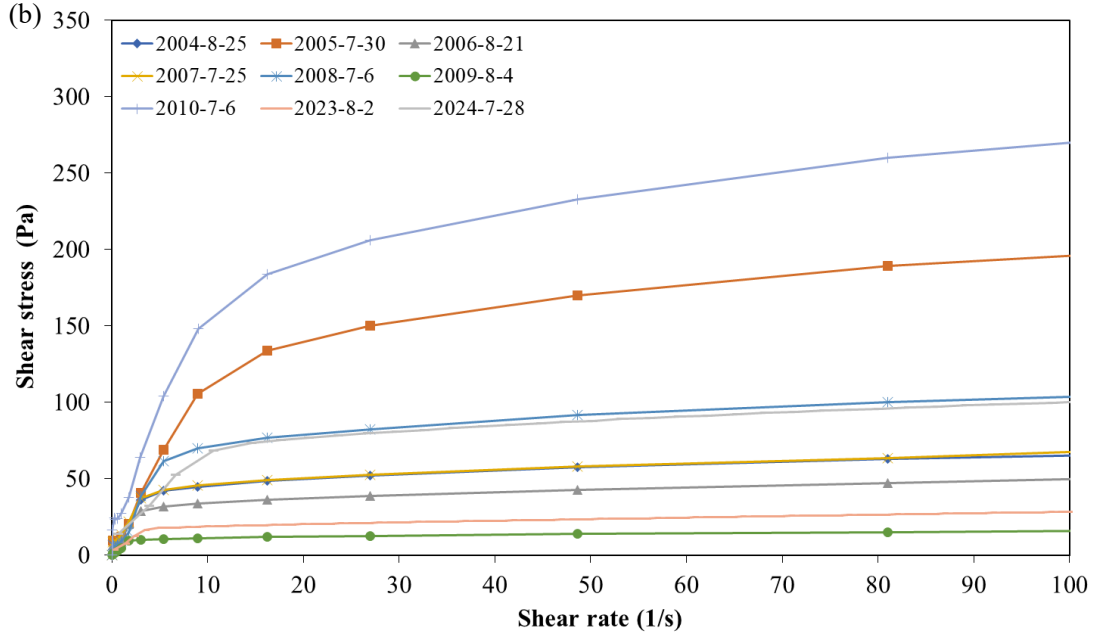
Figure 10. (a) Particle size distribution of debris flow surges occurred during 1974 to 2024 and (b) shear stress of debris-flow slurry occurred during 2004 to 2024.

3.1.4 Debris-flow video footage

Since 2020, high-resolution cameras (3840 × 2160 at 25 fps) have been installed on both sides of the debris-flow channel, including the observation section (Fig.1a). Data is transmitted in real-time through a wireless relay network and can be viewed online via a mobile client APP. These cameras capture real-time footage of debris-flow movements (Fig. 11), which can be used for research of surge flow formation, flow state assessment, and others.

Figure 11. Debris-flow video frames captured on July 28th, 2024: (a) first debris flow surge on coarse bed, (b) surge flow, (c) continuative flow and (d) hyperconcentrated flow.

3.1.5 Cross section elevation

Measurement

To investigate the erosion and deposition resulting from the debris flows, the elevation of various cross-sections was measured after the event. The cross-section elevation was measured using different methods over several decades. From 1962 to 1966, a level gauge was utilized for measurements. In the year 1999 and 2010, measurements were conducted using a total station theodolite. Starting in August 2010, a Real-Time Kinematic (RTK) surveying instrument was employed to measure the cross-section elevation.

Example of results

Figure ~~11~~ 12 presents the change of elevation of cross section M3 from 1999 to 2024. The M3 section is located at the debris flow observation section (Fig.1a). Due to the extremely strong siltation of debris flows, the channel has been raised by 11 m in the past 25 years, with an average annual sedimentation height of 0.44 m. The main channel gradually shifted to the right bank and has become narrower and shallower.
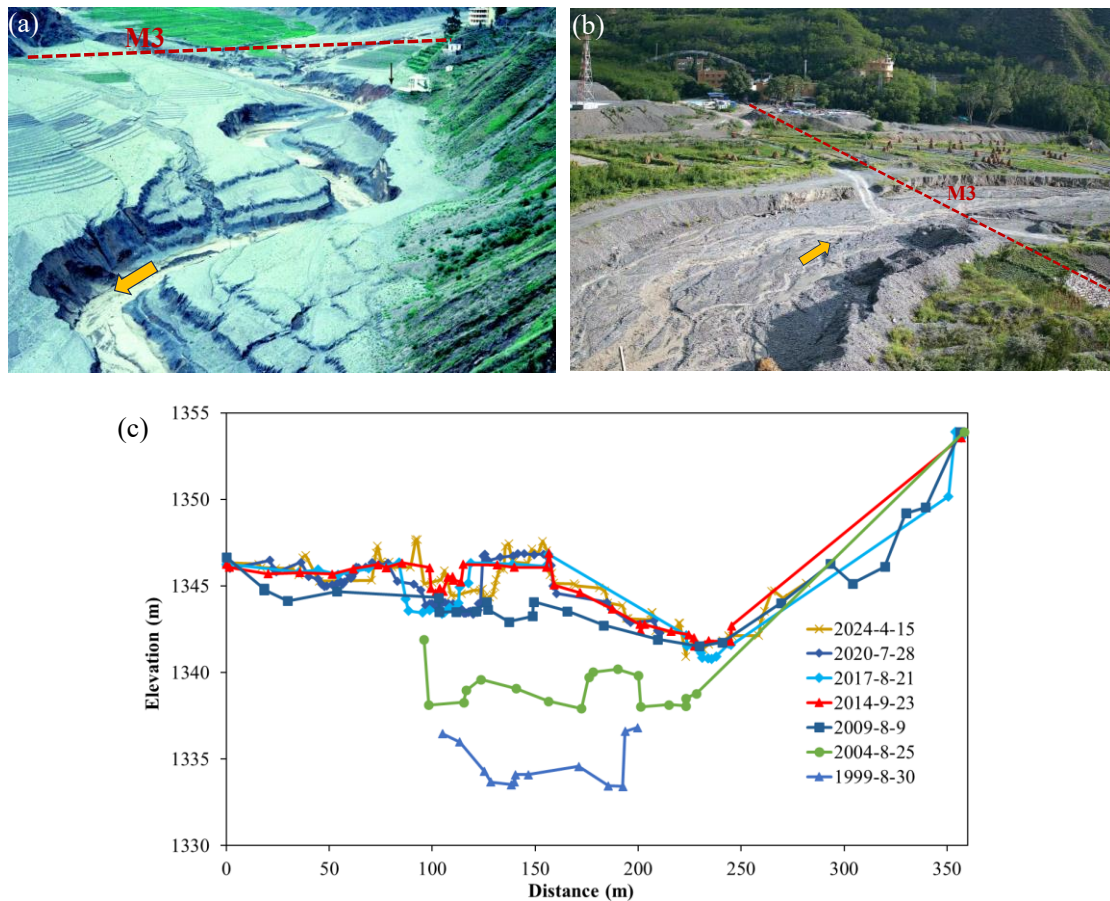

Figure ~~11~~12. (a) Location of cross section M3 in the 1990s (Photo by R.J. Janda), (b) location in 2024 and (c) ~~Change~~ change of elevation of cross section M3 from 1999 to 2024 (from right bank to left bank).

3.2 Atmosphere

3.2.1 Rainfall

Measurement

Before 2006, rainfall was measured using a siphon rain gauge with a measurement range of 0.1 mm

to 10 mm and an error margin of ±0.05 mm. This gauge could measure precipitation intensities from 0.1 mm/10 min to 40 mm/10 min. From 2006 to 2023, rainfall measurements were conducted using a tipping-bucket rain gauge (Fig.12a13a), which had a range of 0-4 mm/min, a minimum measurement increment of 0.1 mm, and a maximum allowable error of ±4%. In 2024, the rainfall was monitored by piezoelectric rain gauges (Fig.12b13b), which had a range of 0-200 mm/h, a minimum measurement increment of 0.1 mm, and a maximum allowable error of ±4%.

Before 2024, the rainfall data are stored in a logger system that records rainfall time. Every 3 months, data are retrieved from the logger, the rain gauge is cleaned if needed (leaves, spider web). The 2024 rainfall data measured by piezoelectric rain gauge was transmitted wirelessly via 4G signals. With a dome-type sensor area, this new type of rain gauge requires no maintenance.

Example of results

Detailed records of rainfall allow for deep research into the imitation mechanism of debris flows. An example of rainfall measured at minute intervals from 01:51 (UTC+8) to 23:00 (UTC+8) on 28th July 2024, at Lijiayakou rain gauge, is shown in Fig. 12c13c. The debris flow occurred at 11:25, when the cumulative rainfall reached 41.2 mm and rainfall intensity computed over 1 min reached 31.6 mm/h. Rainfall records are also aggregated and analyzed on daily scale. The boxplot Fig. 13d illustrates the distribution of monthly rainfall throughout the year. Rainfall shows obvious seasonality, peaking during the rainy season (June to September) and reaching its lowest levels during the dry season (November to March)Figure 12d illustrates the monthly distribution of rainfall at the Mayiping rain gauge over the period from 2013 to 2024. With a total annual rainfall of 827 mm, the heaviest rainfall occurs between June and September.
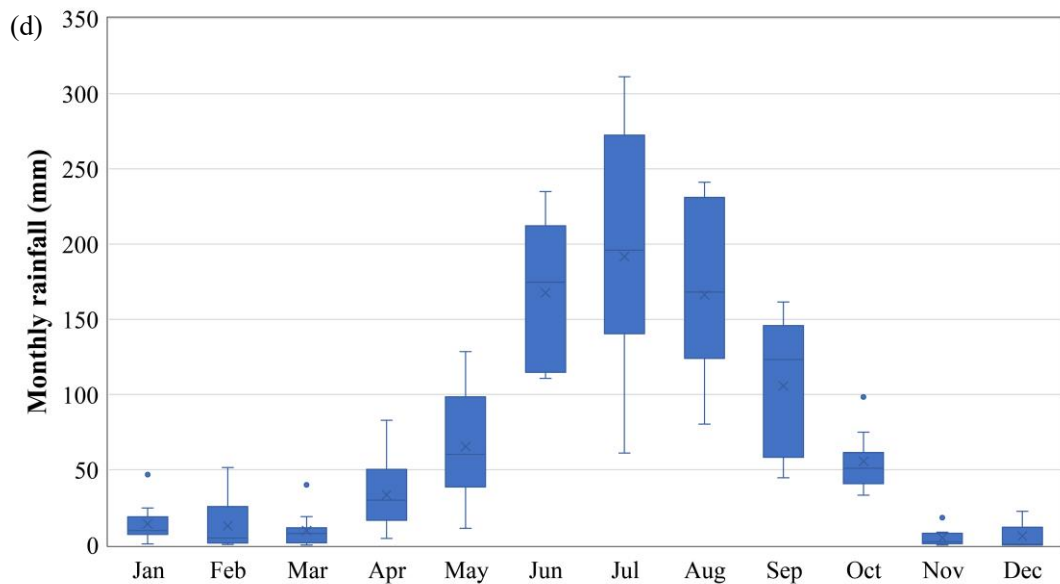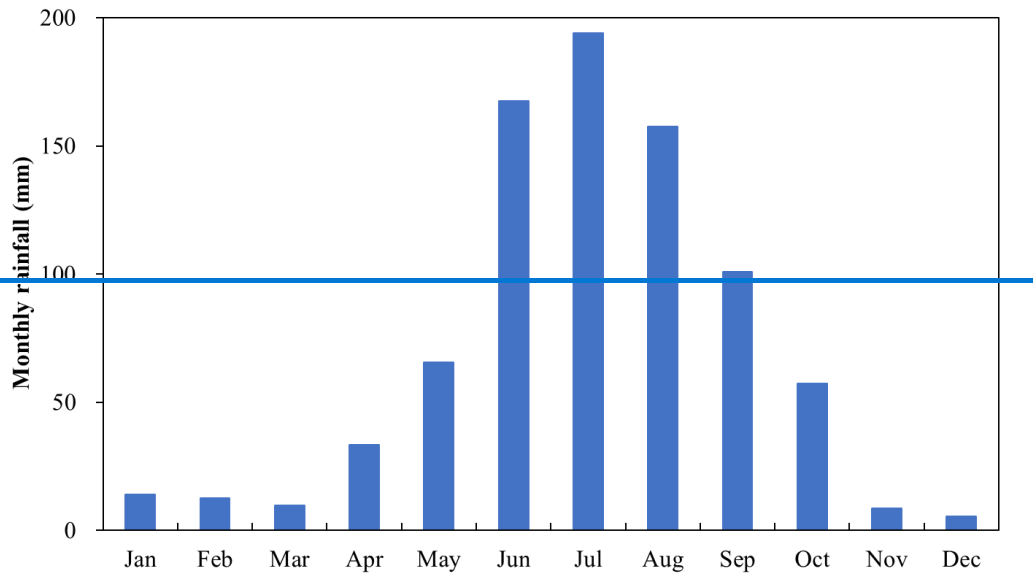
.

(d)
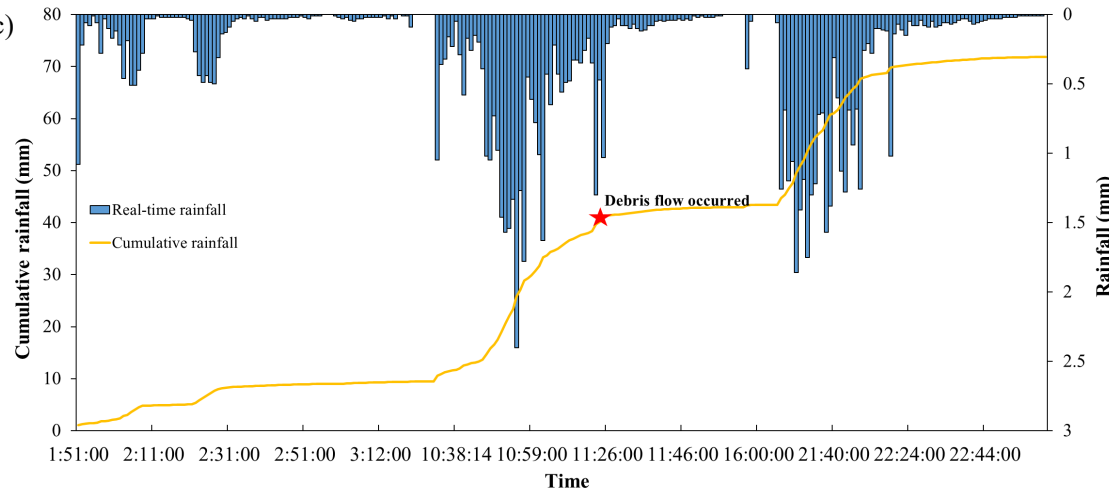
Figure ~~12~~13. (a) Photo of tipping-bucket rain gauge~~,~~. (b) photo of piezoelectric rain gauge~~,~~. (c) real-time and cumulative rainfall at Lijiayakou rain gauge on July 28th, 2024 ~~and~~. (d) statistical box plot of monthly rainfall at the Mayiping rain gauge (rainfall data are averaged over period 2013-2023). The points above the box plot denote extreme monthly rainfall.~~s Monthly rainfall at the Mayiping rain gauge (rainfall data are averaged over period 2013-2023).~~

3.2.2 Meteorology

Measurement

Early in the year 1965, meteorological data for Xiadawa included measurements of air pressure, temperature, relative humidity, soil temperature, wind speed, and rainfall. A Cumulus automatic weather station manufactured by ELE International was installed in 2004 and 2005 at the Observation station and Mayiping Station, respectively. New weather station was installed in 2024 at the Observation station, Mayiping Station, Kuikou Station (See location in Fig. 1a). It includes soil temperature, air temperature, air humidity, wind direction and speed, radiation and pressure. Table 1 summarizes the type of instruments, record interval, accuracy and resolution.

25

Three climatic stations were installed at three locations vary in altitude within the Xiaojiang River Catchment (Nideping station coordinates are 103.11528° and 26.264444°; elevation is 1132 m; Daduo station coordinates are 103.0774° and 26.240339°; elevation is 2030 m; Yinmin station coordinates are 103.01156° and 26.26244°, elevation is 3045 m). The station includes air temperature, air humidity, illuminance, soil moisture and temperature at different depths. Data are stored in a logger system and data are retrieved from the logger every six months.

Example of results

The Xiaojiang River Catchment is a typical dry-hot valley region in southwest China, characterized by a prolonged dry season with low precipitation and high evaporation rates (Jiang et al., 2024). Figure ~~13a~~ 14 illustrates the temporal variation in air temperature at three stations located at different altitudes within the catchment from October 10th to December 13th, 2018. The temperature increases as altitude decreases, with an average temperature difference of 10.4°C between Nideping and Yinmin.
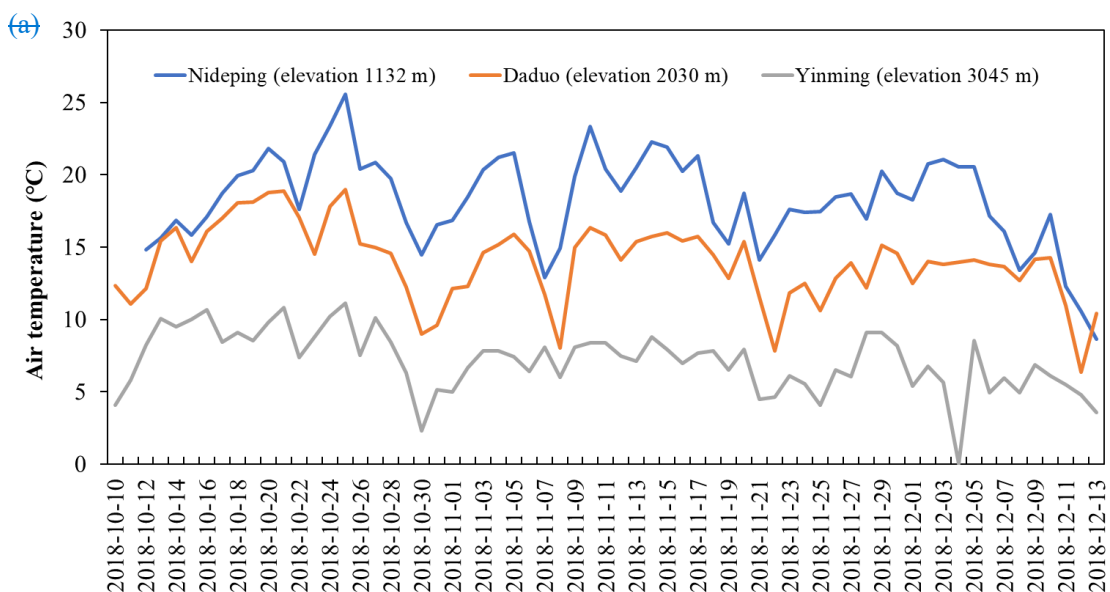
3.2.3 Soil moisture

Measurement

In 1966, soil moisture at a runoff plot (location see Fig.1a) was manually sampled and analyzed using the oven-drying method. From 2017 to 2024, MS-20 sensors were used to monitor soil moisture and temperature at depths of 10 cm, 20 cm, and 30 cm at three locations with wide-graded gravelly soil at Jiangjia Ravine. These sensors provide precise soil moisture measurements across a 0-100% range and temperatures from -40°C to 80°C. The accuracy of moisture measurements varies: ±2% within the 0-53% range and ±4% for values exceeding 53%, up to 100%. Additionally, the sensors offer a temperature measurement accuracy of ±0.4°C.

~~**Example of results**~~

~~Figure 13b illustrates the temporal variation in soil moisture content at different depths at Point 3 on the right bank of Section D3 (location see Fig.1a), measured on July 28th, 2024. The moisture content in the near-surface layer (10 cm depth) was lower than in the deeper layers, with an average difference of 11%. Additionally, the soil moisture content at 20 cm depth was higher than at 30 cm depth. This trend of change may be caused by preferential flow, which were affected by soil porosity characteristics and soil texture.~~
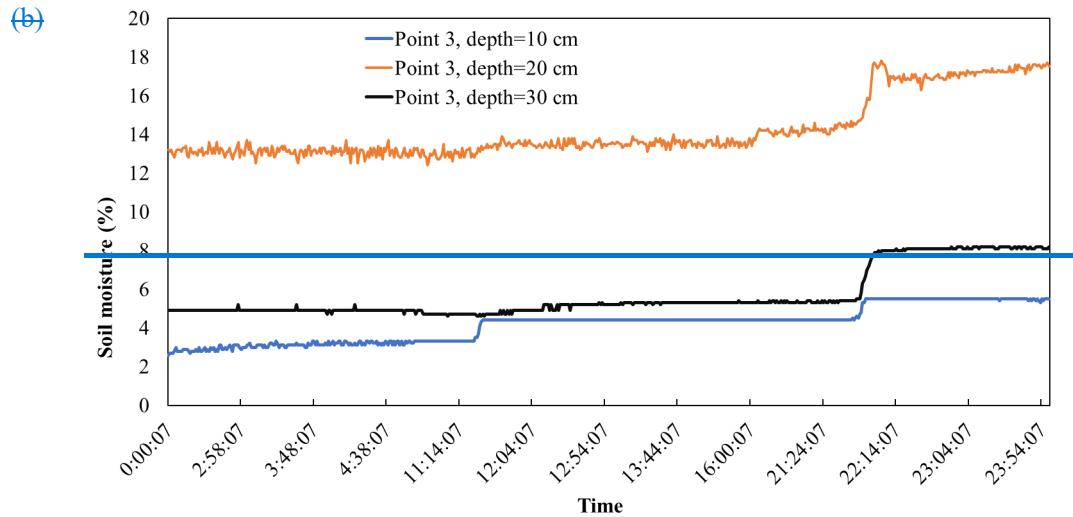
(a)

456
457   **Figure ~~13~~14.** ~~(a)~~Temporal variation of air temperature at Nideping, Daduo, and Yinmin stations from
458   October 10th to December 13th in 2018 and ~~(b)soil moisture of the right bank of Section D3 at Jiangjia~~
459   ~~Ravine on July 28th, 2024.~~

3.3 Runoff and sediment in runoff plot

Measurement

Naturally restored runoff plots and Leucaena leucocephala runoff plots were built near DDFORS in
2005 (Fig.~~14~~15). The runoff plots are 20 m by 5 m in size, and the slope is approximately 22°. In terms
of vegetation coverage, the Leucaena leucocephala runoff plots include Leucaena leucocephala (Lam.)
de Wit, Leucaena leucocephala (Lam.) de Wit and Agave sisalana Perr. ex Engelm, and Leucaena
latisiliqua (L.) Gillis with the crown removed. The naturally restored runoff plots are categorized into
forest land dominated by Leucaena leucocephala, agricultural land, and wasteland. These plots have not
undergone any artificial interventions, and the data are for reference only. Runoff volume is obtained by
measuring the flow volume in the iron bucket. Sediment concentration is obtained by the same method
as mentioned above.

Figure ~~14~~15. Photos of runoff plot: (a) agricultural land runoff plot~~.(~~ and (b) forest land runoff plot

3.4 Suspended sediment at Jiangjia Ravine and Xiaojiang River

Measurement

In 1966, the runoff discharge at Jiangjia Ravine in Baishapo and Xiadawa was estimated based on
manually measured flow area and velocity. From 2004, the suspended-sediment concentration and grain

27

size distribution were measured in Xiaojiang River at different locations. From 2012, the sediment
concentration and sediment grain size distribution of runoff were measured at Jiangjia Ravine. A water
sample was manually collected with a volume of 500 ml, and then sediment contained within the sample
was filtered, dried, and weighed. Sediment concentration was determined by comparing the weight of
the sediment to the total sample weight. Particle size analysis of the sediment was conducted using a
Malvern laser particle size analyzer (Model MS2000).

Example of results

An example of the suspended sediment concentration time series for the Xiaojiang River, obtained
from May 10th to December 3rd 2007 at the Gele station (103.0611438°, 26.53562376°), is presented in
Fig.15a16a. The highest concentration, 43 kg/m³, was observed on 13th July. The concentration varied
significantly between July 11th and September 23rd, a period characterized by frequent debris flows in
the Xiaojiang River catchment, which transported large amounts of sediment to the main river. Figure
15b 16b also illustrates the variation in suspended sediment concentration at Jiangjia Ravine between
June 9th and August 20th, with the highest concentration, 628 kg/m³, observed on June 30th.
Concentrations exceeding 628 kg/m³ were consistently recorded following debris-flow events when
floods carried additional sediment and caused a significant increase in sediment concentration.
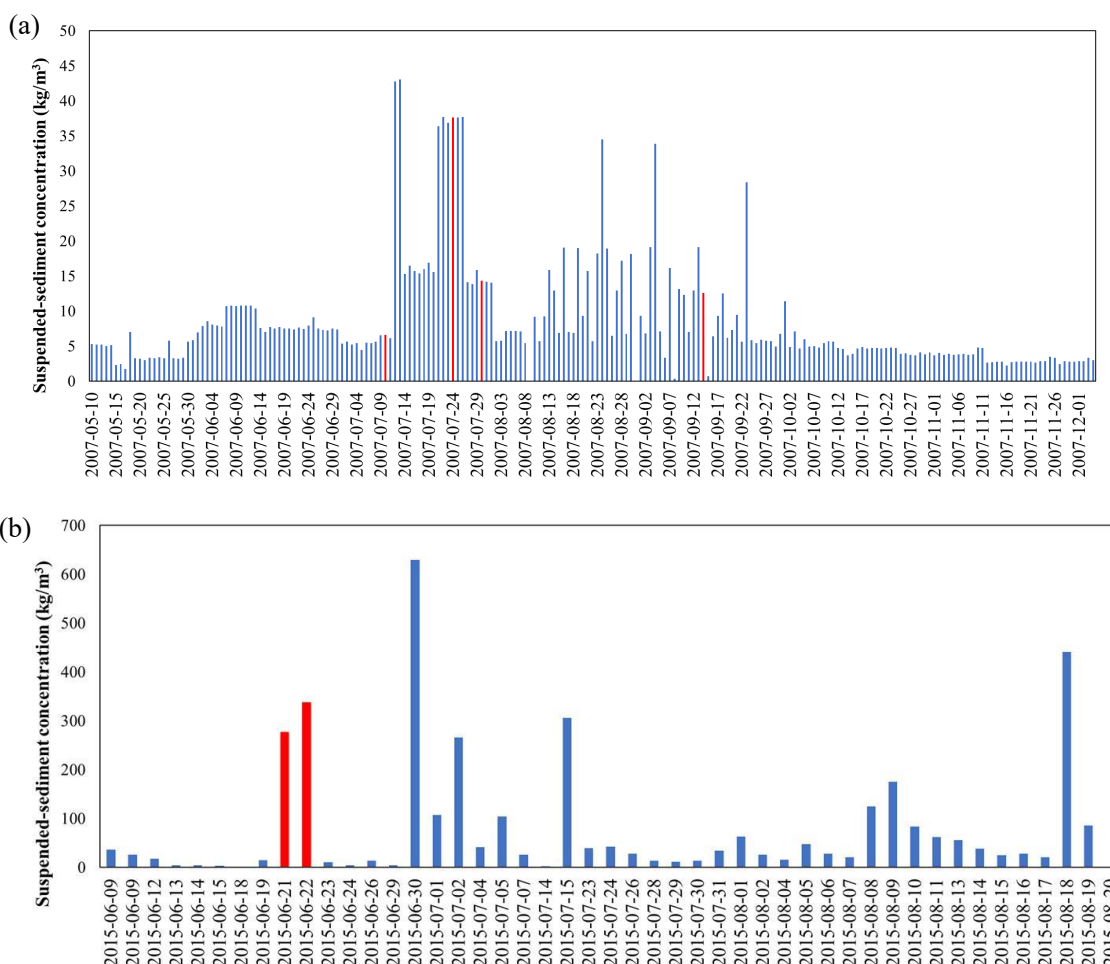

Figure 1516. Suspended sediment concentration variation: (a) Xiaojiang River at Gele station in 2007
and (b) Jiangjia Ravine in 2015. The red bars represent water samples collected after the debris-flow
event at Jiangjia Ravine.

28

Most datasets, including debris-flow kinematic data, particle size distribution of debris flows, rheological data of debris-flow slurry, cross-sectional measurement data, sediment concentration, grain size distribution data, and observation data from runoff plots, were obtained through manual observation. These data are considered to have relatively small errors. Additionally, rainfall data from tipping-bucket rain gauges, collected prior to 2024, showed high reliability when cross-validated with data from regional national meteorological stations. In 2024, piezoelectric rain gauges and meteorological stations were installed and underwent performance verification at national benchmark sites before deployment. The correlation coefficients between these instruments and the reference data from national meteorological stations were 0.951 for the piezoelectric rain gauges and 0.996 for the meteorological stations.

4. Examples of studies and open questions

This debris-flow dataset is valuable for analyzing the dynamic behavior, deposition, and erosion characteristics of debris flows. Several studies are presented to demonstrate the dataset's potential and to elicit the open questions.

4.1 Debris-flow dynamic characteristics

The comprehensive records of debris-flow depth, velocity, density, and discharge enable the analysis of dynamic characteristics of debris flows and the comparison of various computational models (Wu, 1987; Hu et al., 2011; Hu et al., 2013; Tian et al., 2014; Zhu et al., 2020; Chen et al., 2023; Chen et al., 2024). In the early 1980s, based on observational data at Jiangjia Ravine, the Chinese researchers modified the Manning formula for velocity and resistance calculation of viscous (high solid-concentration) debris flows. These formulas have been widely applied in the design of debris-flow mitigation structures across China (Chen and Wang, 1983; Kang, 1984, 1987, 1990,2004; China Geological Disaster Prevention Engineering Association, 2018a, 2018b; Kwan, 2012). Additionally, Zhang (1993) reported that the impact pressure of debris flows obeys the conservation of momentum (proportional to the unit weight and the square of the flow velocity), while the impulse load of boulders within debris flows varies with the stiffness of the exposed elements.

The flow-depth time history (e.g., Fig. 6a) provides solid evidence for verification of dynamic models. Chen et al. (2024) adopted the surge-depth hydrographs measured by ultrasonic sensors (1999-2001) to quantify the eroded deposition depth of surge flows (see Fig. 4c). For surge flows with erosion-deposition propagation, significant downward erosion potential is confirmed. Therefore, the total momentum of surge flow not only originates from the apparent surge front, but also includes the momentum within the eroded deposition layer. The revealed erosion pattern and hidden momentum in debris-flow surges may improve the reliability of debris-flow risk assessment.

Based on 5,085 debris-flow measurements collected from Jiangjia Ravine between 1990 and 2001, along with 1,035 measurements from catchments across Asia, America, Europe, and Oceania, Du et al. (2023) established a criterion for distinguishing debris flows, hyperconcentrated flows, and stream flows. Their findings indicate that sediments in hyperconcentrated flows and stream flows are primarily supported by viscous shear and turbulent stresses, whereas grain collisional stresses play a dominant role in debris-flow dynamics. The study identifies flow discharge and sediment flux as key factors differentiating debris flows, hyperconcentrated flows, and stream flows.

4.2 The non-hydrostatic pore fluid pressure

Current research, integrating field observations (McArdell et al., 2007; Nagl et al., 2020) and flume experiments (Cassar et al., 2005; Iverson et al., 2010; Kaitna et al., 2014; Song et al., 2021, 2023), has

recognized the non-hydrostatic pore fluid pressure, notably excess pore fluid pressure, in debris flows. However, direct measurement of basal normal stress, shear stress, and pore fluid pressure at Jiangjia Ravine remains impractical, due to challenges posed by erosion, deposition, and channel migration. To circumvent these limitations, Chen et al. (2023) proposed a simplified analytical method to estimate debris-flow liquefaction. By assuming steady-state flow on a 3.7° slope and neglecting particle collision-induced resistance, they attributed flow resistance primarily to Coulomb friction regulated by pore fluid pressure and liquid-phase viscosity. Analysis of 93 debris-flow events (1999-2017) revealed near-liquefaction conditions, with degree of liquefaction ranging from 0.89 to 0.95. Therefore, with the consideration of particle collision-induced resistance, the degree of liquefaction would be even higher (close to unity). This finding demonstrates that analysis relying on hydrostatic pore fluid pressure assumptions to infer grain-contact stresses (i.e., effective stresses) are invalid. Such approach, initially introduced by Iverson (1997) to calculate dimensionless parameters (e.g., Savage number, friction number) for debris flows, have been largely abandoned in light of direct pore fluid pressure and effective stress measurements (Iverson et al., 2010). As a result, we caution against the derivation of flow regime characteristics (by dimensionless parameters) from observational datasets lacking direct basal stress measurements.

4.3 Surge flow characteristics and surge flow formation

Debris flows at Jiangjia Ravine propagate as surge waves (roll waves), comprising dozens to hundreds of intermittent surges. Discharge values within a surge series (1966-2004) follow an exponential cumulative distribution, with exponents scaling as a power-law function of peak discharge (Liu et al., 2009). This implies that the mean discharge evolves dynamically during the surge sequence, ultimately decaying via a power-law relationship. Surge velocities in 1994 conform to a Weibull distribution, characterized by stable parameters across events, where the shape parameter correlates with mean velocity (Li et al., 2012). Similarly, the peak discharge-frequency relationship for surges (1987-2004) adheres to a Weibull distribution (Chen et al., 2011), while the magnitude-cumulative frequency relationship aligns with either an exponential function or a linear logarithmic transformation (Liu et al., 2008; Gao et al., 2019). Notably, discharge fluctuations within individual events span four orders of magnitude, with sediment transport variability diminishing in a power-law manner as surges progress (Liu et al., 2023).

The debris-flow surge waves carry much higher momentum flux than the continuative flows in the same debris-flow event, posing higher destructive potential to the infrastructures. The formation of surge flows is currently one of the hot research topics of debris-flow dynamics. The discontinuous sediment supply is regarded as a potential explanation of surge flows. The formation of intermittent surges arises from shallow slope failures distributed across broad source areas rather than discrete large landslides. These failures can be modeled using a Pareto-Poisson process (PPP model), where the intensity parameter is governed by rainfall dynamics in source regions (Guo et al., 2023). Through captured processes by video camera at Chalk Cliffs, Kean et al. (2013) attributed the surge flow formation by upstream variations in channel slope. The low-gradient sections act as "sediment capacitors," temporarily storing incoming bed load transported by water flow and periodically releasing the accumulated sediment as debris surges. This "store-release" pattern is also observed in the small branch gullies of Jiangjia Ravine. However, this pattern may not explain the surge behavior in the main channel, which is characterized by high degree of liquefaction. Further understanding of the surge flow formation, on one hand, relies on the intense and precise instrumentation in the debris-flow source area (e.g., processes

583   captured by video cameras), on the other hand, benefits from the development of granular-fluid flow
584   models (Meng et al., 2022).

4.4 Debris-flow grain composition

586   The effect of particle size on debris-flow behavior is a fundamental question. Previous research
587   framework adopted specific particle parameters to distinguish clay, silt, sand, and gravel. Based on
588   particle size distribution data from debris flows in Jiangjia Ravine, Li et al. (2013) developed a
589   generalized grain size distribution model defined by parameters closely linked to key dynamical
590   properties, including flow density, velocity, and discharge. Subsequent studies demonstrate that grain
591   composition imposes power-law constraints on debris-flow surge fluctuations (Li et al., 2014), while
592   debris-flow density and cumulative sediment yield adhere to a unified sediment size distribution
593   framework (Wang et al., 2018; Liu et al., 2023；Zhang et al.,2025). Observations reveal a progressive
594   increase in fine particles and a corresponding decline in coarse particles during intermittent flow
595   sequences, alongside reductions in median grain diameter, bimodality parameters, and mass density.
596   viscous particle content in continuous flows increases incrementally, whereas mass density exhibits a
597   pronounced decrease (Wei and Hu, 2014).

4.5 Debris flow erosion and deposition characteristics

599   Between 1966 and 1973, the debris-flow channel at Jiangjia Ravine experienced substantial erosion
600   and deposition due to viscous (high solid fraction) debris flows. The average annual scouring depth in
601   the upper reaches was 2-3 m, while the average annual deposition depth in the lower reaches was 2-2.5
602   m (Kang, 1997). During this period, a single debris-flow event could erode the channel bed to a depth of
603   2-3 m, and sometimes even 8-10 m (Li et al., 1983). From 1999 to 2003, the relatively lower magnitudes
604   of debris flows led to sediment deposition in the majority of the river sections. However, the increasing
605   annual sediment discharge resulted in a reduction of deposition in the upper reaches and an enhancement
606   of deposition in the lower reaches (Chen et al., 2005). Wei et al. (2017) reported that, between 1999 and
607   2009, channel width increased significantly, stabilizing after 2009 when erosion and deposition intensity
608   decreased. From 2003 to 2014, the gradient of the channel profile experienced a gradual increase,
609   eventually reaching 0.07, although the rate of increase slowed after 2009. Debris flows were primarily
610   characterized by siltation in the transportation zone, with variations across different sections. The middle
611   and upper reaches experienced greater siltation, while the middle and lower reaches underwent more
612   substantial scouring (Fang et al., 2018). Overall, from 1962 to 2024, the channel has undergone
613   significant siltation. The underlying causes of this channel aggradation may be related to climate change
614   induced reduction in debris-flow frequency or long-term geomorphic evolution controlled by the tectonic
615   activities.

4.6 Rainfall threshold triggering debris flows

617   Detailed rainfall records have enabled the investigation of rainfall threshold in debris-flow
618   forecasting. 167 debris-flow events at Jiangjia Ravine occurred at night (from 19:00 to 07:00 of the next
619   day), accounting for 58.4% (Chen et al., 2025). Debris flows are primarily triggered by intraday
620   precipitation lasting 6 hours or less, while antecedent precipitation is not a significant factor, the
621   Intensity-Duration (I-D) thresholds for debris flows at 50%, 70%, and 90% probabilities have been
622   determined (Zhuang et al., 2015). In contrast, Rainfall threshold for triggering debris flows do not
623   consistently decrease with increasing antecedent effective precipitation (AEP). In fact, higher AEP may
624   require more stringent triggering conditions (Zhang et al., 2023). The relationship between the
625   probability of a debris flow and AEP can be quantified using a piecewise function. When 10 mm ≤ AEP

≤ 85 mm, the rainfall I-D threshold curves can be described by an exponential function. This indicates that higher soil water content allows solid material from shallow landslides to become readily available without prolonged rainfall infiltration, and a high soil water content in the topsoil facilitates rapid runoff generation (Zhang et al., 2024). Yang et al. (2024) demonstrated that models using maximum rainfall intensity over short durations and absolute energy are the most effective predictors for debris-flow occurrence. Adding rainfall duration or antecedent rainfall to these models further improves their performance.

The intermittent failure of shallow landslides makes the rainfall-induced debris flows at Jiangjia Ravine even complicated. Guo et al. (2020) revealed that a debris flow is the product of a rainfall-induced "normal" or "abnormal" hydrological process involving the supply of soil materials. They argued that although various types of debris flows may require similar rainfall conditions, the threshold for debris-flow initiation can be expressed as a power function, and that the threshold could be expressed as power function. Debris flows are more closely related to rainfall patterns than to rainfall amounts, typically occurring within 6 hours of a rainfall event characterized by high mean intensity and short duration. However, the formation type, process, and discharge of debris flows show no direct relationship with rainfall amount. These findings highlight the significance of soil supply in debris flow formation through random disturbances to the normal hydrological process. Additionally, Guo et al. (2021) demonstrated that interpolation errors decrease with higher rainfall amounts, while the representativeness of rain gauges diminishes when the distance between gauges exceeds 3 km. The influence of climate change such as changes in precipitation intensity and frequency, and changes in temperature on the triggering mechanisms of debris flows at Jiangjia Ravine requires further analysis.

For a more comprehensive list of data-based research papers, please refer to https://nsl.imde.ac.cn/en/publ/article_2020/.

5. Data availability

The debris flow, atmospheric, runoff, and sediment data, including the suspended sediment concentration and particle size in the Xiaojiang River, are publicly accessible through the National Cryosphere Desert Data Center (NCDC) (https://www.ncdc.ac.cn/). The dataset is organized into 11 categories: dynamic parameters of debris flow, seismic data, particle size distribution of debris flow sediment, yield stress and viscosity of debris-flow slurry, debris-flow video footage, cross-sectional elevation of the debris flow channel, rainfall, meteorological data, soil moisture, runoff and sediment data in runoff plots, and suspended sediment concentration (Table 34). Detailed descriptions of the measurement methods, data collection locations, and data processing techniques are included for each category. All data files are provided in China Standard Time (CST, UTC+8).

This debris-flow dataset will be updated using newly collected measure data at a one-year interval. The updated dataset will continue to be released freely and publicly on the National Cryosphere Desert Data Center (NCDC).

Table 3 4 Dataset categories and open repository.

Dataset	Data DOI	Reference
Debris-flow kinematic data	http://dx.doi.org/10.12072/ncdc.ddfors.db6803.2025	Song et al., 2025a
Seismic data of debris flow	http://dx.doi.org/10.12072/ncdc.ddfors.db6804.2025	Song et al., 2025b
Particle size distribution of debris flows	http://dx.doi.org/10.12072/ncdc.ddfors.db6721.2025	Song et al., 2025c
Rheological data of debris-	http://dx.doi.org/10.12072/ncdc.ddfors.db6720.2025	Song et al., 2025d

flow slurry		
Debris-flow video	http://dx.doi.org/10.12072/ncdc.ddfors.db6807.2025	Song et al., 2025e
Cross-sectional measurement data	http://dx.doi.org/10.12072/ncdc.ddfors.db6719.2025	Song et al., 2025f
Meteorological data	http://dx.doi.org/10.12072/ncdc.ddfors.db6805.2025	Song et al., 2025g
Rainfall data	http://dx.doi.org/10.12072/ncdc.ddfors.db6716.2025	Song et al., 2025h
Soil moisture and temperature data	http://dx.doi.org/10.12072/ncdc.ddfors.db6718.2025	Song et al., 2025i
Sediment concentration and grain size distribution data	http://dx.doi.org/10.12072/ncdc.ddfors.db6802.2025	Song et al., 2025j
Observation data at runoff plots	http://dx.doi.org/10.12072/ncdc.ddfors.db6806.2025	Song et al., 2025k

6. Conclusion

We present a comprehensive dataset of debris-flow and hydrometeorological observations collected from 1961 to 2024 at Jiangjia Ravine. This collection encompasses detailed measurements of kinematic parameters (such as debris-flow velocity, depth, and surge discharge) and physical-mechanical parameters (including particle size, yield stress, and viscosity), along with seismic data. In addition, it features extensive records of rainfall, soil moisture, and suspended sediment concentrations at the catchment scale. The breadth of this documentation supports rigorous analyses of debris-flow initiation, transport, and deposition, while highlighting the crucial role of hydrometeorological conditions particularly rainfall in triggering debris flows. Furthermore, the suspended sediment concentration data provides valuable insights into sediment transport within mountainous watersheds prone to frequent debris-flow events. The dataset is also useful for the research of influence of climate change on debris-flow occurrence, tectonic-disaster-geomorphic evolution. Overall, this dataset constitutes a vital resource with significant potential to advance both theoretical and practical research on debris-flow processes.

Author contribution

DS designed the framework of this research; LW, XG, CS and HT performed the data analyses and wrote the manuscript; ZK, JZ, GO, PC, FW, KH, LS, GZ, DS, WZ, YZ contributed to data collection; YH and XL installed and maintained the instruments and infrastructures.

Competing interests

The corresponding author declares that none of the authors has any competing interests.

Acknowledgements

691   others colleagues of Dongchuan Debris Flow Observation and Research Station (DDFORS), Chinese

692   Academy of Sciences, who contribute to the field observation of Jiangjia Ravine debris flows since the

693   year 1961.

Reference

Aaron, J., Spielmann, R., McArdell, B.W., Graf, C.: High-frequency 3D LiDAR measurements of a debris flow: A novel method to investigate the dynamics of full-scale events in the field, Geophysical Research Letters,50, e2022GL102373. https://doi.org/10.1029/2022GL102373, 2023.

Abancó, C., Hürlimann, M., Moya, J.: Analysis of the ground vibration produced by debris flows and other torrential processes at the Rebaixader monitoring site (Catalan Pyrenees, Spain), Nat Hazards Earth Syst Sci 14:929–943. https://doi.org/10.5194/nhess-14-929-2014, 2014.

Bel, C., Navratil, O., Liébault, F., Fontaine, F., Bellot, H., Laigle, D.: Monitoring debris flow propagation in steep erodible channels, In: Lollino G, Arattano M, Rinaldi M, Giustolisi O, Marechal J.-C, Grant GE (eds) Engineering geology for society and territory, vol. 3. Springer International Publishing, 103-107, https://doi.org/10.1007/978-3-319-09054-2_20, 2015.

Berger, C., McArdell, B., Schlunegger, F.: Direct measurement of channel erosion by debris flows, Illgraben, Switzerland, J. Geophys. Res.,116, F01002, doi:10.1029/2010JF001722, 2011.

Berti, M., Genevois, R., La Husen, R., Simoni, A., Tecca, P.R.: Debris flow monitoring in the Acquabona watershed on the Dolomites (Italian Alps), Phys. Chem. Earth 25, 707–715, https://doi.org/10.1016/S1464-1909(00)00090-3, 2000.

Berti, M., Genevois, R., Simoni, A., Tecca, P.R.: Field observations of a debris flow event in the Dolomites, Geomorphology, 29(3), 265-274, https://doi.org/10.1016/S0169-555X(99)00018-5, 1999.

Blasone, G, Cavalli, M, Cazorzi, F.: Debris-flow monitoring and geomorphic change detection combining laser scanning and fast photogrammetric surveys in the Moscardo catchment (Eastern Italian Alps), In: Lollino G, Arattano M, Rinaldi M, Giustolisi O., Marechal J, Grant GE (eds) Engineering geology for society and territory, Springer, 3, 51–54, https://doi.org/10.1007/978-3-319-09054-2_10, 2015.

Cassar, C., Nicolas, M., & Pouliquen, O.: Submarine granular flows down inclined planes. Physics of Fluids, 17(10), 103301, https://doi.org/10.1063/1.2069864, 2005.

Chen, J., He, Y. P., Wei, F. Q.: Debris flow erosion and deposition in Jiangjia gully, Yunnan, China, Environmental Geology, 48(6), 771-777, https://doi.org/10.1007/s00254-005-0017-z, 2005.

Chen, J.W.: A Preliminary Analysis of the Relation Between Debris Flow and Rainstorm at Jiangjia Gully of Dongchuan in Yunnan, Memoris of Lanzhou Institute of Glaciology and Cryopedology Chinese Academy of Science, 4,88-96, https://doi.org/10.3133/pp1671,1985.

Chen, N.S., Yang, C.L., Zhou, W., Wei F.Q., Li, Z.L., Han, D., Hu, G.S.: A new total volume model of debris flows with intermittent surges: based on the observations at Jiangjia Valley, southwest China, Natural hazards, 56(1), 37-57, https://doi.org/10.1007/s11069-010-9548-z, 2011.

Chen, Q., Song, D., Chen, X., Feng, L., Li, X., Zhao, W., Zhang, Y.: The erosion pattern and hidden momentum in debris-flow surges revealed by simple hydraulic jump equations, Water Resources Research, 60, e2023WR036090. https://doi.org/10.1029/ 2023WR036090, 2024.

Chen, Q., Song, D., Chen, X., Zhong, W.: Visco-collisional scaling law of flow resistance and its application in debris-flow mobility, Journal of Geophysical Research: Earth Surface, 128, e2022JF006712. https://doi.org/10.1029/2022JF006712, 2023.

Chen, Q., Song, D., Wei, L., Jiang H, Tang, H., Wang, Y.: The nocturnal occurrence of debris flows: evidence from western China, npj Natural Hazards, 2(58), 1-15,https://doi.org/10.1038/s44304-025-00114-22025, 2025.

Chen, G.X., Wang, J.K.: Debris Flow Prevention and Control, China Railway Publishing House, 71-80,1983.

China geological disaster prevention engineering association: Specification of Design for Debris Flow Prevention (T/CAGHP 021-2018), 2018a.

China geological disaster prevention engineering association: Specification of Geological Investigation for Debris Flow Stabilization (T/CAGHP 006-2018), 2018b.

Coe, J., Kean, J., Mccoy, Scott., Staley, D., Wasklewicz, T.: Chalk Creek Valley: Colorado's natural debris-flow laboratory, in Geol. Soc. Am. Field Guides, 18, 95–117, https://doi.org/10.1130/2010.0018(05), 2010.

Comiti, F., Marchi, L., Macconi, P., Arattano, M., Bertoldi, G., Borga, M., Brardinoni, F., Cavalli, M., D'Agostino, V., Penna, D., Theule, J.: A new monitoring station for debris flows in the European Alps: first observations in the Gadria basin, Nat. Hazards, 73, 1175–1198, https://doi.org/10.1007/s11069-014-1088-5, 2014.

Coviello, V., Arattano, M., Turconi, L.: Detecting torrential processes from a distance with a seismic monitoring network, Nat. Hazards 78, 2055–2080 https://doi.org/10.1007/s11069-015-1819-2, 2015

Cui, P., Chen, X.Q., Wang, Y. Y., Hu, K.H., Li, Y.: Jiangjia Ravine debris flows in south-western China, In: Jakob M, Hungr O (eds) Debris-flow hazards and related phenomena. Springer, Berlin, 2005.

Du, J., Zhou, G. G. D., Tang, H., Turowski, J. M., Cui, K. F. E.: Classification of stream, hyperconcentrated, and debris flow using dimensional analysis and machine learning, Water Resources Research, 59, e2022WR033242. https://doi.org/10.1029/2022WR033242, 2023.

Fan, X., Scaringi, G., Domènech, G., Yang, F., Guo, X., Dai, L., He, C., Xu, Q., and Huang, R.: Two multi-temporal datasets that track the enhanced landsliding after the 2008 Wenchuan earthquake, Earth Syst. Sci. Data, 11, 35-55, https://doi.org/10.5194/essd-11-35-2019, https://doi.org/10.5194/essd-11-35-2019, 2019.

Fand, Y.C., Wang, D.J., He, S.T., Lan, H.J., Chang, S.Q.: Characteristics of Debris Flow Erosion and Deposition at Jiangjia Gully, Dongchuan,Yunnan Province, China for 2003-2014, Mountain Research, 36(6),907-916, https://doi.org/10.16089 /j.cnki.1008-2786. 00038, 2018.

Fuchs, S., Ornetsmüller, C. &, Totschnig, R. Spatial scan statistics in vulnerability assessment: an application to mountain hazards. Nat Hazards, 64, 2129–2151. https://doi.org/10.1007/s11069-011-0081-5,2012

Gao, Y. C., Chen, N.S., Hu, G.S., Deng, M.F: Magnitude-frequency relationship of debris flows in the Jiangjia Gully, China, Journal of Mountain Science, 16(6). https://doi.org/10.1007/s11629-018-4877-6, 2019.

Genevois, R, Tecca, P, Breti, M, Simoni, A.: Debris-flow in the dolomites: experimental data from a monitoring system, In: Wieczorek GF, Naeser ND (eds) Debris-flow hazards mitigation: mechanics, prediction, and assessment, Proceedings of the 2nd international conference, Balkema Press, Taipei, Taiwan, Rotterdam, 283-291, 16-18, 2000

Guo, X. J., Su, F. H., Hong, Y., Zou, Q.: Characteristics of hydrogen and oxygen isotopes in rainy season precipitation in Jiangjiagou Watershed, Research of Soil and Water Conservation, 19, 2, 82-85, 2012.

Guo, X.J., Cui, P., Chen, X.C., Li Y., Zhang, J., Sun, Y.Q.: Spatial uncertainty of rainfall and its impact on hydrological hazard forecasting in a small semiarid mountainous watershed, Journal of Hydrology, 595,126049, https://doi.org/10.1016/j.jhydrol.2021.126049, 2021.

Guo, X.J., Li Y., Chen, X.C., Zhang, J., Sun, Y.Q.: Variation of debris flow/flood formation conditions at the watershed scale in the Wenchuan Earthquake area, Landslides. 18. 1-17. 10.1007/s10346-021-01644-2, 2021.

Guo, X.J., Li, Y., Cui, P., Yan, H., Zhuang, J.Q.: Intermittent viscous debris flow formation in Jiangjia Gully from the perspectives of hydrological processes and material supply, Journal of Hydrology, 589. 125184, https://doi.org/10.1016/j.jhydrol.2020.125184, 2020.

Guo, X.J., Li, Y., Yao, Y.J., et al.: A Pareto-Poisson process model for intermittent debris flow surges developing from slope failures, Eng Geol, 314, 106998, https://doi.org/10.1016/j.enggeo.2023.106998, 2023.

Hirschberg, J., Fatichi, S., Bennett, G. L., McArdell, B. W., Peleg, N., Lane, S. N., Schlunegger, F., Molnar, P.: Climate change impacts on sediment yield and debris flow activity in an Alpine catchment, Journal of Geophysical Research: Earth Surface, 126, e2020JF005739. https:// doi.org/10.1029/2020JF005739, 2021.

Hirschberg, J., McArdell, B. W., Mirus, B. B.: Volumetric Water Content Measurements at Illgraben 2022, EnviDat.

https://www.doi.org/10.16904/envidat.489, 2024.

Hu, K. H., Hu, C., Li, Y., Cui, P.: Characteristics and mechanism of debris-flow surges at Jiangjia Ravine, In: Genevois R, Hamilton DL, Prestininzi A (eds) 5th international conference on debris-flow hazards mitigation: mechanics, prediction and assessment, 211-217, https://www.doi.org/10.4408/IJEGE.2011-03.B-025, 2011.

Hu, K.H., Wei, F.Q., Li, Y.: Real-time measurement and preliminary analysis of debris-flow impact force at Jiangjia Ravine, China, Earth Surface Processes and Landforms, https://doi.org/36.1268-1278. 10.1002/esp.2155, 2011.

Hübl, J., Kaitna, R.:Sediment delivery from the Lattenbach catchment by debris floods and debris flows, EGU General Assembly. 10585. 2-7 May 2010, Vienna, Austria, 10585, 2010.

Hübl, J., Mikoš, M.: Practice guidelines on monitoring and warning technology for debris flows, In: Sassa, K., Guzzetti, F., Yamagishi, H., Arbanas, Ž., Casagli, N., McSaveney, M., Dang, K. (Eds.), Landslide Dynamics: ISDR-ICL Landslide Interactive Teaching Tools. Springer Nature, 567–585, https://doi.org/10.1007/978-3-319-57774-6_41, 2018.

Hübl, J., Moser, M.: Risk management in Lattenbach: a case study from Austria, In: Lorenzi G, Brebbia C, Emmanouloudis D (eds) Monitoring. Simulation, prevention and remediation of dense and debris flows, WIT Press, Southamption, 333-342, https://doi.org/10.2495/DEB060321, 2006.

Hübl, J., Schimmel, A., Koschuch, R.: Monitoring of debris flows with an improved system setup at the lattenbach catchment, austria. Springer, Cham, https://www.doi.org/10.1007/978-3-319-53485-5_53, 2017.

Hürlimann, M., Abancó, C., Moya, J., Raïmat, C., Luis-Fonseca, R.: Debris-flow monitoring stations in the Eastern Pyrenees. Description of instrumentation, first experiences and preliminary results, In: Genevois, R., Hamilton, D., Prestininzi, A. (Eds.), 5th International Conference on Debris-Flow Hazards Mitigation. Casa Editrice Universita La Sapienza, Padua, 553-562, https://www.doi.org/10.4408/IJEGE.2011-03.B-061, 2011.

Hürlimann, M., Abancó, C., Moya, J.: Experiences of Debris-Flow Monitoring and Warning at Catchment Scale in the Pyrenees, Landslide Science and Practice: Early Warning, Instrumentation and Monitoring, 2, 153-159. https://www.doi.org/10.1007/978-3-642-31445-2-20, 2013.

Hürlimann, M., Coviello, V., Bel, C., Guo, X.J., Berti, M., Graf, C., Hübl, J., Miyata, S., Smith, J. B., Yin, H.Y., Debris-flow monitoring and warning: Review and examples, Earth-Science Reviews, 199, 102981, https://doi.org/10.1016/j.earscirev.2019.102981, 2019.

Hürlimann, M., McArdell, W.B., Rickli, C.: Field and laboratory analysis of the runout characteristics of hillslope debris flows in Switzerland, Geomorphology, 232, 20-32, https://www.doi.org/10.1016/j.geomorph.2014.11.030, 2015.

Ikeda, A., Itoh, T., Mizuyama, T.: Study of debris flow peak discharge at Kamikamihorizawa Creek, 8th International Conference on Debris Flow Hazard Mitigation (DFHM8) E3S Web of Conferences 415, 03012, https://doi.org/10.1051/e3sconf/202341503012, 2023.Arattano, M., Marchi, L.: Systems and sensors for debris-flow monitoring and warning. Sensors 8, 2436-2452, https://doi.org/10.3390/s8042436, 2008.

Iverson, R. M.: The physics of debris flows, Reviews of Geophysics, 35(3), 245-296. https://doi.org/10.1029/97RG00426, 1997.

Iverson, R.M., Logan, M., Lahusen, R.G., Berti, M.: The perfect debris flow? Aggregated results from 28 large-scale experiments, Journal of Geophysical Research, 115(F3), https://doi.org/10.1029/2009JF001514, 2010.

Jiang, H., Chen, X.Q., Li, Y.P., Chen, J.G., Wei, L., Zhang, Y.B.: Seasonal dynamics of soil microbiome in response to dry-wet alternation along the Jinsha River Dry-hot Valley, BMC Microbiology, 24, 496, https://doi.org/10.1186/s12866-024-03662-1, 2024.

Kaitna, R., Dietrich, W.E., Hsu, L.: Surface slopes, velocity profiles and fluid pressure in coarse-grained debris flows saturated with water and mud, Journal of Fluid Mechanics, 741, 377-403, https://doi.org/10.1017/jfm.2013.675, 2014.

825   Kang, Z.C. : A velocity research of debris flow and it's calculation method in China, Mountain Research, 5(4), 247-
826   259, https://doi.org/10.16089/j.cnki.10082786.1987.04.012, 1987.

827   Kang, Z.C., Cui P., Wei F.Q., He S.F.: Data collection of kinematic observation of debris flows in Jiangjia Ravine,
828   Dongchuan, Yunnan (1995-2000). Beijing: Science Press, 2007.

829   Kang, Z.C., Cui, P., Wei, F.Q., He, S.F.: Data collection of kinematic observation of debris flows in Jiangjia Ravine,
830   Dongchuan, Yunnan (1961-1984). Beijing: Science Press, 2006.

831   Kang, Z.C., Li, Z.F., Ma, A.N., Luo, J.T.: Research on Debris Flows in China, Science Press, Beijing, 2004.

832   Kang, Z.C: Motion Characteristics of Debris Flow at Jiangjia Gully, Yunnan Province, China, International Research
833   and Training Center on Erosion and Sedimentation (IRTCES), 1-38, 1990.

834   Kang, Z.C: Topographic Change in the Stream Channel by Viscous Debris Flow, Annuals of disasters prevention
835   Research Institution, Kyoto University,40,167-172, 1997.

836   Kang,Z.C.: An analysis of maximum discharge of viscous debris flow at Jiangjia Gully of Dongchuan in Yunnan, In:
837   Memoirs of Lanzhou Institute of Glaciology and Cryop edology, Chinese Academy of Sciences(4),
838   Beijing,Science Press, 108-118, 1984.

839   Kean, J.W., McCoy, S.W., Tucker, G.E., Staley, D.M, Coe, J.A.: Runoff-generated debris flows: observations and
840   modeling of surge initiation, magnitude, and frequency, J Geophys Res-Earth, 118(4), 2190–2207,
841   https://doi.org/10.1002/jgrf.20148, 2013.

842   Kwan J.S.H.: Supplementary technical guidance on design of rigid debris-resisting barriers, GEO Report No. 270.
843   Geotechnical Engineering Office, HKSAR Government, 2012.

844   LaHusen, R.: Debris-flow instrumentation. In: Jakob, M., Hungr, O. (Eds.), Debris- Flow Hazards and Related
845   Phenomena, Springer, Berlin, 291-304, 2005

846   Lapillonne, S., Fontaine, F., Liebault, Frédéric., Richefeu, V., Piton, G., Debris-flow surges of a very active alpine
847   torrent: a   field   database,   Natural   Hazards   and   Earth   System   Sciences.   23,1241-125,
848   https://www.doi.org/10.5194/nhess-23-1241-2023, 2023.

849   Li, J., Wu, J.N.: An Analysis on the Formation Condition of Debris Flows in the Jingjia Gully, Dongchuan, Yunna.:
850   Collected Papers on Debris Flows, Chongqing Branch of Science and Technology Press, 26-29, 1981..

851   Li, J., Yuan, J., Bi, C., Luo, D.: The main features of the mudflow in Jiang-Jia Ravine, Zeitschrift für Geomorphologie,
852   27(3), 325-341 https://doi.org/10.1127/zfg/27/1983/325, 1983.

853   Li, Y., Liu, J.J., Hu, K.H., Su, P.C.: Probability distribution of measured debris-flow velocity in Jiangjia Gully,
854   Yunnan Province, China, Nat Hazards, 60, 689-701, https://doi.org/10.1007/s11069-011-0033-0, 2012.

855   Li, Y., Liu, J.J., Su, F.H., Xie, J., Wang, B.L.: Relationship between grain composition and debris flow characteristics:
856   a case study of the Jiangjia Gully in China, Landslides, 12, https://doi.org/10.1007/s10346-014-0475-z, 2014.

857   Li, Y., Zhou, X.J. , Su, P.C. , Kong, Y.D., Liu, J.J.: A scaling distribution for grain composition of debris flow,
858   Geomorphology, 192,30–42, https://doi.org/10.1016/j.geomorph.2013.03.015, 2013.

859   Liu, D.C., Jia, Y., He, Y.Y., Shao, Jiang, X.B., Liang, M., Wang, F.M., Guo, C.C..: Spatial-temporal characteristics
860   of sediment transport by intermittent surges, Landslides. 1-17. https://doi.org/10.1007/s10346-023-02025-7,
861   2023.

862   Liu, J.J., Li, Y., Su, P.C., Cheng, Z.L., Cui, P.: Temporal variation of intermittent surges of debris flow, J. Hydrol.,
863   365(3–4), 322–328, https://doi.org/10.1016/j.jhydrol.2008.12.005, 2009.

864   Liu, J.J., Li,Y., Su, P. C. , Cheng, Z.L. :Magnitude-frequency relations in debris flow, Environmental Geology, 55(6),
865   1345-1354, https://doi.org/10.1007/s11629-018-4877-6, 2008.

866   Liu, K.F., Wei, S.C.: Real-time debris flow monitoring and automated warning system, Journal of Mountain Science,
867   21, 4050-4061. 10.1007/s11629-024-9269-5, 2024.

868   Marchi, L., Arattano, M., Deganutti, A.M., Ten years of debris-flow monitoring in the Morcardo Torrent (Italian

869   Alps), Geomorphology 46, 1-17, http://dx.doi.org/10.1016/ S0169-555X (01)00162-3, 2002.

870   Marchi, L., Cazorzi, F., Arattano, M., Cucchiaro, S., Cavalli, M., and Crema, S.: Debris flows recorded in the
871   Moscardo catchment (Italian Alps) between 1990 and 2019, Nat. Hazards Earth Syst. Sci., 21, 87–97,
872   https://doi.org/10.5194/nhess-21-87-2021, 2021.

873   Marchi, L., Crema, S.: Data on debris-flow volumes in northeastern Italy [dataset], PANGAEA,
874   https://doi.org/10.1594/PANGAEA.896595, 2018.

875   McArdell, B. W. and Hirschberg, J.: Debris-flow volumes at the Illgraben 2000-2017, EnviDat [data set],
876   https://doi.org/10.16904/envidat.173, 2020.

877   McArdell, B. W., Hirschberg, J., Graf, C., Boss, S., Badoux, A.: Illgraben debris-flow characteristics 2019-2022,
878   EnviDat. https://doi.org/10.16904/envidat.378, 2023.

879   McArdell, B. W., Hirschberg, J.: Debris-flow volumes at the Illgraben 2000-2017, EnviDat.
880   https://doi.org/10.16904/envidat.173, 2020.

881   McArdell, B.W., Bartelt, P., Kowalski, J.: Field observations of basal forces and fluid pore pressure in a debris flow,
882   Geophysical Research Letters, 340, https://doi.org/10.1029/2006GL029183, 2007.

883   McArdell, B.W., Bartelt, P., Kowalski, J.: Field observations of basal forces and fluid pore pressure in a debris flow,
884   Geophysical Research Letters, 34, L07406, https://doi.org/10.1029/2006GL029183, 2007.

885   Mccoy, S.W., Coe, J.A., Kean, J.W., Tucker, G.E., Staley, D.M., Wasklewicz, T. A., Sediment entrainment by debris
886   flows: In situ measurements from the headwaters of a steep catchment, J. Geophys. Res., 117, F03016,
887   https://doi.org/10.1029/2011JF002278, 2012.

888   Mccoy, S.W., Coe, J.A., Kean, J.W., Tucker, G.E., Staley, D.M., Wasklewicz, T. A.: Observations of debris flows at
889   Chalk Cliffs, Colorado, USA: Part 1, In situ measurements of flow dynamics, tracer particle movement and
890   video imagery from the summer of 2009, Ital. J. Eng. Geol. Environ., https://doi.org/1. 10.4408/IJEGE.2011-
891   03. B-078, 2011.

892   McCoy, S.W., Kean, J.W., Coe, J.A., Staley, D.M., Wasklewicz, T.A., Tucker, G.E.: Evolution of a natural debris
893   flow: in situ measurements of flow dynamics, video imagery, and terrestrial laser scanning, Geology 38:735–
894   738. https://doi.org/10.1130/G30928.1, 2010.

895   Meng X., Johnson C.G., Gray J.M.N.T.: Formation of dry granular fronts and watery tails in debris flows, Journal
896   of Fluid Mechanics, 943, A19. https://doi.org/10.1017/jfm.2022.400, 2022.

897   Mitchell, A., Jacquemart, M., Hübl, J., Kaitna, R., Graf, C.: Debris flow discharge hydrographs from Dorfbach &
898   Spreitgraben, Switzerland, and Lattenbach, Austria [dataset], PANGAEA,
899   https://doi.org/10.1594/PANGAEA.943970, 2022.

900   Nagl, G., Hübl, J., Kaitna, R.: Velocity profiles and basal stresses in natural debris flows, Earth Surf. Process.
901   Landforms, 45, 1764-1776, https://doi.org/10.1002/esp.4844, 2020.

902   Navratil, O., Liébault, F., Bellot, H., Travaglini, E., Theule, J., Chambon, G., Laigle, D.: High-frequency monitoring
903   of debris-flows propagation in the Réal Torrent, Southern French Alps, Geomorphology. 201.
904   10.1016/j.geomorph.2013.06.017, 2013.

905   Okano, K., Suwa, H., Kanno, T.: Characterization of debris flows by rainstorm condition at a torrent on the Mount
906   Yakedake volcano, Japan, Geomorphology, 136 (1),88-94, https://doi.org/10.1016/j.geomorph.2011.04.006,
907   2012.

908   Pierson, T.C.: Flow behavior of channelized debris flows, Mount St. Helens, Washington. In: Abrahms AD (ed)
909   Hillslope processes, Allen & Unwin, Boston, 269-296, https://doi.org/10.4324/9781003028840-13, 1986.

910   Raffaele, S., Jordan, A.: A new method for detailed discharge and volume measurements of debris flows based on
911   high-frequency 3D LiDAR point clouds; Illgraben, Switzerland, Engineering Geology,329,107386,
912   https://doi.org/10.1016/j.enggeo.2023.107386, 2024.

Riekenmann, D., McArdell, B. W.: Continuous measurement of sediment transport in the Erlenbach stream using piezoelectric bedload impact sensors, Earth. Surf. Proc. Land., 32, 1362–1378, https://doi.org/10.1002/esp.1478, 2007.

Scott, K.M., Wang, Y.Y.: Debris flows: geologic process and hazard; illustrated by a surge sequence at Jiangjia Ravine, Yunnan, China, Reston, VA: Retrieved from USGS Publications Warehouse Retrieved from http://pubs.er.usgs.gov/publication/pp1671, 2004.

Song, D.R., Chen, X. Q., Sadeghi, H., Zhong, W., Hu, H., Liu, W.: Impact behavior of dense debris flows regulated by pore-pressure feedback, Journal of Geophysical Research: Earth Surface, 128(12), e2023JF007074, https://doi.org/10.1029/2023JF007074, 2023.

Song, D.R., Chen, X.Q., Gordon G.D. Zhou, Lu, X.Q., Cheng, G.W., Chen, Q.: Impact dynamics of debris flow against rigid obstacle in laboratory experiments, Engineering Geology, 291, 106211, https://doi.org/10.1016/j.enggeo.2021.106211, 2021.

Song D.R., Zhong W., Li X.Y., Wei L.: Debris-flow kinematic data at Jiangjia Ravine, Dongchuan, Yunnan, China, from 1961 to 2024, National Cryosphere Desert Data Center(http://www.ncdc.ac.cn), https://www.doi.org/10.12072 /ncdc. ddfors.db6803.2025, 2025a.

Song D.R., Zhong W., Li X.Y., Wei L.: Seismic data of debris flow at Jiangjia Ravine, Yunnan, China, from 2023 to 2024, National Cryosphere Desert Data Center(http://www.ncdc.ac.cn), https://www.doi.org/10.12072/ncdc. ddfors.db6804.2025, 2025b.

Song D.R., Zhong W., Li X.Y., Wei L.: Particle size distribution of debris flows at Jiangjia Ravine, Dongchuan, Yunnan, China, in 1965, 1966, 1974, 1975, 1982, and from 2003 to 2024, National Cryosphere Desert Data Center(http://www.ncdc.ac.cn), https://www.doi.org/10.12072/ncdc.ddfors.db6721.2025, 2025c.

Song D.R., Zhong W., Li X.Y., Wei L.: Rheological data of debris-flow slurry at Jiangjia Ravine, Yunnan, China, from 2003 to 2024, National Cryosphere Desert Data Center(http://www.ncdc.ac.cn), https://www.doi.org/10.12072/ncdc.ddfors.db6720.2025 2025d.

Song D.R., Zhong W., Li X.Y., Wei L.: Video of debris flows that occurred in 2023 and 2024 at Jiangjia Ravine, Dongchuan, Yunnan, China, National Cryosphere Desert Data Center(http://www.ncdc.ac.cn), https://www.doi.org/10.12072/ncdc.ddfors.db6807.2025 2025e.

Song D.R., Zhong W., Li X.Y., Wei L.: Cross-sectional measurement data at Jiangjia Ravine, Yunnan, China, National Cryosphere Desert Data Center(http://www.ncdc.ac.cn), https://www.doi.org/ 10.12072/ncdc.ddfors. db6719.2025, 2025f.

Song D.R., Zhong W., Li X.Y., Wei L.: Meteorological data at Jiangjia Ravine and Xiaojiang River Catchment, Yunnan, China, National Cryosphere Desert Data Center (http://www.ncdc.ac.cn), https://www.doi.org/ 10.12072/ncdc.ddfors.db6805.2025, 2025g.

Song D.R., Zhong W., Li X.Y., Wei L.: Rainfall data at Jiangjiag Ravine and Xiaojiang River Catchment, Yunnan, China, National Cryosphere Desert Data Center (http://www.ncdc.ac.cn), https://www.doi.org/10.12072/ncdc. ddfors.db6716.2025, 2025h.

Song D.R., Zhong W., Li X.Y., Wei L.: Soil moisture and temperature data at Jiangjia Ravine, Yunnan, China, from 2017 to 2024, National Cryosphere Desert Data Center (http://www.ncdc.ac.cn), https://www.doi.org/10.12072/ ncdc.ddfors.db6718.2025, 2025i.

Song D.R., Zhong W., Li X.Y., Wei L.: Sediment concentration and grain size distribution of runoff water sample at Jiangjia Ravine and Xiangjiang River, National Cryosphere Desert Data Center(http://www.ncdc.ac.cn), https://www.doi.org/10.12072/ncdc.ddfors.db6802.2025, 2025j.

Song D.R., Zhong W., Li X.Y., Wei L.: Observation data at runoff plots at Jiangjia Ravine，Yunnan, China, National Cryosphere Desert Data Center (http://www.ncdc.ac.cn), https://www.doi.org/ 10.12072/ncdc.ddfors.

957   db6806.2025 2025k.

958   Suwa, H., Okano, K., Kanno, T.: Forty years of debris-flow monitoring at Kamikamihorizawa Creek, Mount
959   Yakedake, Japan, In: Genevois, R., Hamilton, D.L., Prestininzi, A. (Eds.), Proceedings of the 5th International
960   Conference on Debris Flow Hazards Mitigation, Mechanics, Prediction and Assessment, 605–613,
961   https://doi.org/10.4408/IJEGE.2011-03.B-066, 2011.

962   Suwa, H., Okunishi, K., Sakai, M.: Motion, debris size and scale of debris flows in a valley on Mount Yakedake,
963   Japan, IAHS Publ. no. 217, 1993; pp. 239-248 Proc. international symposium, Yokohama, 1993.

964   Theule, J. I., Crema, S., Marchi, L., Cavalli, M., Comiti, F.: Exploiting LSPIV to assess debris-flow velocities in the
965   field, Nat. Hazards Earth Syst. Sci., 18, 1-13, https://doi.org/10.5194/nhess-18-1-2018, 2018.

966   Theule, J.I., Liébault, F., Laigle, D., Loye, A., Jaboyedoff, M.: Channel scour and fill by debris flows and bedload
967   transport, Geomorphology, 243:92-105, https://doi.org/10.1016/j.geomorph.2015.05.003, 2015.

968   Tobler, D., Kull, I., Jacquemart, M., Haehlen, N: Hazard Management in a Debris Flow Affected Area: Case Study
969   from Spreitgraben, Switzerland. In: Sassa, K., Canuti, P., Yin, Y. (eds) Landslide Science for a Safer
970   Geoenvironment. Springer, Cham. https://doi.org/10.1007/978-3-319-04996-0_5, 2014.

971   Tian, M., Hu, K.H., Ma, C., Lei, F.H: Effect of Bed Sediment Entrainment on Debris-Flow Resistance, Journal of
972   Hydraulic Engineering, 140. 115-120, ttps://doi.org/10.1016/10.1061/(ASCE)HY.1943-7900.0000805, 2014.

973   Wang, B., Li, Y., Liu, D., et al.: Debris flow density determined by grain composition, Landslides, 15, 1205–1213,
974   https://doi.org/10.1007/s10346-017-0912-x, 2018.

975   Wang, L., Chang, M., Le, J., Xiang, L.L., Ni, Z.: Two multi-temporal datasets to track debris flow after the 2008
976   Wenchuan earthquake, Scientific data, 9, 525, 1-9, https://doi.org/10.1038/s41597-022-01658-y, 2022.

977   Wei, L., Hu, K.H., Li, X.Y., Yan, C.D.: Inter-annual Variation of the Morphology of Debris Flow Channel in Jiangjia
978   Gully, Journal of Yangtze River Scientific Research Institute, 34(9):57-62,
979   https://doi.org/10.11988/ckyyb.20160528, 2017.

980   Wei, L., Hu, K.H.: Study on sediment transporting characteristics of intermittent debris flows in Jiangjia Ravine,
981   Journal of natural disasters, 23(2), 53-60, https://doi.org/10.13577 /j.jnd.2014. 0208, 2014.

982   Willi, C., Graf, C., Deubelbeiss, Y., Keiler, M.: Methods for detecting channel bed surface changes in a mountain
983   torrent – experiences from the Dorfbach torrent, Geogr. Helv., 70, 265–279, https://doi.org/10.5194/gh-70-
984   265-2015, 2015.

985   Wu, J.S., Kang, Z.C., Tian, L.Q.: Observation and Research on Debris Flows in Jiangjia Ravine, Yunnan, Beijing:
986   Science Press, 1990.

987   Wu. J.S.: Fluid state of debris flow in the Jiangjia Ravine, Mountain Research,5(4), 237-246, 1987.

988   Yang, H.J., Zhang, S.J., Hu, K.H., et al.: Field observation of debris-flow activities in the initiation area of the Jiangjia
989   Gully, Yunnan Province, China, Journal of Mountain Science, 19(6), 1602-1617,
990   https://doi.org/10.1007/s11629-021-7292-3, 2022.

991   Yang, H.J., Zhang, S.J., Hu, K.H., Wei, F.Q., Liu, Y.H.: Evaluation of rainfall threshold models for debris flow
992   initiation in the Jiangjia Gully, Yunnan Province, China, J. Mt. Sci. 21, 1799–1813,
993   https://doi.org/10.1007/s11629-023-8507-6, 2024.

994   Yin, H.Y., Huang, C.J., Chen, C.Y., Fang, Y.M., Lee, B.J., Chou, T.Y.: The present development of debris flow
995   monitoring technology in Taiwan-a case study presentation, In: Genevois, R., Hamilton, D., Prestininzi, A.
996   (Eds.), 5th International Conference on Debris-Flow Hazards Mitigation. Casa Editrice Universita La Sapienza,
997   Padua, pp. 623-631, https://doi.org/10.4408/IJEGE.2011-03.B-068, 2011.

998   Zhang J., Xiong G.: Data collection of kinematic observation of debris flows in Jiangjia Ravine, Dongchuan, Yunnan
999   (1987-1994), Beijing: Science Press, 1997.

1000   Zhang, M., Li, Y., Cui, Y.F., Wu, Z., Xue, Y., Cheng, J.Y., Jiang, H., Li, Y., Guo, J. Nie, J.Y., Wang, G.D. Luo, A.:

Unity of terrestrial and extraterrestrial soils in granular configuration, Earth and Planetary Science Letters, 654, 119239, https://doi.org/10.1016/j.epsl.2025.119239, 2025.

Zhang, S.C.: A comprehensive approach to the observation and prevention of debris flows in China, Nat. Hazards, 7(1),1-23,1993.

Zhang, S.C., Hong Y., Yu, B.: Detecting infrasound emission of debris flow for warning purposes, Internationals Symposium INTERPRAEVENT 2004-RIVA/TRIENT, 359-360, 2004

Zhang, S.J., Lei, X.H., Yang, H.J., Hu, K.H., Ma, J., Liu, D.L., Wei, F.Q.: Investigation of the functional relationship between antecedent rainfall and the probability of debris flow occurrence in Jiangjia Gully, China, Hydrology and Earth System Sciences, 28, 2343-2355, https://doi.org/10.5194/hess-28-2343-2024, 2024.

Zhang, S.J., Xia, M.Y., Li, L., Yang, H.J., Liu, D.L., Wei, F.Q.: Quantify the effect of antecedent effective precipitation on rainfall intensity-duration threshold of debris flow, Landslides, 20, 1719–1730, https://doi.org/10.1007/s10346-023-02066-y, 2023.

Zhu, X.H., Liu, B.X., Liu, Y. New Method for Estimating Roughness Coefficient for Debris Flows, Water, 12(9), 2341. https://doi.org/10.3390/w12092341, 2020.

Zhuang, J. Q., Cui, P., Wang, G. H., Chen, X. Q., Iqbal, J., and Guo, X. J.: Rainfall thresholds for the occurrence of debris flows in Jiangjia Gully, Yunnan Province, China, Eng. Geol., 195, 335–346, http://dx.doi.org/10.1016/j.enggeo.2015.06.006, 2015.